# Search for gravitational waves from Scorpius X-1 with a hidden Markov model in O3 LIGO data

R. Abbott et al. (LIGO Scientific Collaboration, Virgo Collaboration, and KAGRA Collaboration)

Phys. Rev. D **106**, 062002 — Published 21 September 2022

DOI: 10.1103/PhysRevD.106.062002

# Search for gravitational waves from Scorpius X-1 with a hidden Markov model in O3 LIGO data

R. Abbott,[1] H. Abe,[2] F. Acernese,[3,4] K. Ackley,[5] N. Adhikari,[6] R. X. Adhikari,[1] V. K. Adkins,[7] V. B. Adya,[8] C. Affeldt,[9,10] D. Agarwal,[11] M. Agathos,[12,13] K. Agatsuma,[14] N. Aggarwal,[15] O. D. Aguiar,[16] L. Aiello,[17] A. Ain,[18] P. Ajith,[19] T. Akutsu,[20,21] S. Albanesi,[22,23] R. A. Alfaidi,[24] A. Allocca,[25,4] P. A. Altin,[8] A. Amato,[26] C. Anand,[5] S. Anand,[1] A. Ananyeva,[1] S. B. Anderson,[1] W. G. Anderson,[6] M. Ando,[27,28] T. Andrade,[29] N. Andres,[30] M. Andrés-Carcasona,[31] T. Andrić,[32] S. V. Angelova,[33] S. Ansoldi,[34,35] J. M. Antelis,[36] S. Antier,[37,38] T. Apostolatos,[39] E. Z. Appavuravther,[40,41] S. Appert,[1] S. K. Apple,[42] K. Arai,[1] A. Araya,[43] M. C. Araya,[1] J. S. Areeda,[44] M. Arène,[45] N. Aritomi,[20] N. Arnaud,[46,47] M. Arogeti,[48] S. M. Aronson,[7] H. Asada,[49] Y. Asali,[50] G. Ashton,[51] Y. Aso,[52,53] M. Assiduo,[54,55] S. Assis de Souza Melo,[47] S. M. Aston,[56] P. Astone,[57] F. Aubin,[55] K. AultONeal,[36] C. Austin,[7] S. Babak,[45] F. Badaracco,[58] M. K. M. Bader,[59] C. Badger,[60] S. Bae,[61] Y. Bae,[62] A. M. Baer,[63] S. Bagnasco,[23] Y. Bai,[1] J. Baird,[45] R. Bajpai,[64] T. Baka,[65] M. Ball,[66] G. Ballardin,[47] S. W. Ballmer,[67] A. Balsamo,[63] G. Baltus,[68] S. Banagiri,[15] B. Banerjee,[32] D. Bankar,[11] J. C. Barayoga,[1] C. Barbieri,[69,70,71] B. C. Barish,[1] D. Barker,[72] P. Barneo,[29] F. Barone,[73,4] B. Barr,[24] L. Barsotti,[74] M. Barsuglia,[45] D. Barta,[75] J. Bartlett,[72] M. A. Barton,[24] I. Bartos,[76] S. Basak,[19] R. Bassiri,[77] A. Basti,[78,18] M. Bawaj,[40,79] J. C. Bayley,[24] M. Bazzan,[80,81] B. R. Becher,[82] B. Bécsy,[83] V. M. Bedakihale,[84] F. Beirnaert,[85] M. Bejger,[86] I. Belahcene,[46] V. Benedetto,[87] D. Beniwal,[88] M. G. Benjamin,[89] T. F. Bennett,[90] J. D. Bentley,[14] M. BenYaala,[33] S. Bera,[11] M. Berbel,[91] F. Bergamin,[9,10] B. K. Berger,[77] S. Bernuzzi,[13] D. Bersanetti,[92] A. Bertolini,[59] J. Betzwieser,[56] D. Beveridge,[93] R. Bhandare,[94] A. V. Bhandari,[11] U. Bhardwaj,[38,59] R. Bhatt,[1] D. Bhattacharjee,[95] S. Bhaumik,[76] A. Bianchi,[59,96] I. A. Bilenko,[97] G. Billingsley,[1] S. Bini,[98,99] R. Birney,[100] O. Birnholtz,[101] S. Biscans,[1,74] M. Bischi,[54,55] S. Biscoveanu,[74] A. Bisht,[9,10] B. Biswas,[11] M. Bitossi,[47,18] M.-A. Bizouard,[37] J. K. Blackburn,[1] C. D. Blair,[93] D. G. Blair,[93] R. M. Blair,[72] F. Bobba,[102,103] N. Bode,[9,10] M. Boër,[37] G. Bogaert,[37] M. Boldrini,[104,57] G. N. Bolingbroke,[88] L. D. Bonavena,[80] F. Bondu,[105] E. Bonilla,[77] R. Bonnand,[30] P. Booker,[9,10] B. A. Boom,[59] R. Bork,[1] V. Boschi,[18] N. Bose,[106] S. Bose,[11] V. Bossilkov,[93] V. Boudart,[68] Y. Bouffanais,[80,81] A. Bozzi,[47] C. Bradaschia,[18] P. R. Brady,[6] A. Bramley,[56] A. Branch,[56] M. Branchesi,[32,107] J. E. Brau,[66] M. Breschi,[13] T. Briant,[108] J. H. Briggs,[24] A. Brillet,[37] M. Brinkmann,[9,10] P. Brockill,[6] A. F. Brooks,[1] J. Brooks,[47] D. D. Brown,[88] S. Brunett,[1] G. Bruno,[58] R. Bruntz,[63] J. Bryant,[14] F. Bucci,[55] T. Bulik,[109] H. J. Bulten,[59] A. Buonanno,[110,111] K. Burtnyk,[72] R. Buscicchio,[14] D. Buskulic,[30] C. Buy,[112] R. L. Byer,[77] G. S. Cabourn Davies,[51] G. Cabras,[34,35] R. Cabrita,[58] L. Cadonati,[48] M. Caesar,[113] G. Cagnoli,[26] C. Cahillane,[72] J. Calderón Bustillo,[114] J. D. Callaghan,[24] T. A. Callister,[115,116] E. Calloni,[25,4] J. Cameron,[93] J. B. Camp,[117] M. Canepa,[118,92] S. Canevarolo,[65] M. Cannavacciuolo,[102] K. C. Cannon,[28] H. Cao,[88] Z. Cao,[119] E. Capocasa,[45,20] E. Capote,[67] G. Carapella,[102,103] F. Carbognani,[47] M. Carlassara,[9,10] J. B. Carlin,[120] M. F. Carney,[15] M. Carpinelli,[121,122,47] G. Carrillo,[66] G. Carullo,[78,18] T. L. Carver,[17] J. Casanueva Diaz,[47] C. Casentini,[123,124] G. Castaldi,[125] S. Caudill,[59,65] M. Cavaglià,[95] F. Cavalier,[46] R. Cavalieri,[47] G. Cella,[18] P. Cerdá-Durán,[126] E. Cesarini,[124] W. Chaibi,[37] S. Chalathadka Subrahmanya,[127] E. Champion,[128] C.-H. Chan,[129] C. Chan,[28] C. L. Chan,[130] K. Chan,[130] M. Chan,[131] K. Chandra,[106] I. P. Chang,[129] P. Chanial,[47] S. Chao,[129] C. Chapman-Bird,[24] P. Charlton,[132] E. A. Chase,[15] E. Chassande-Mottin,[45] C. Chatterjee,[93] Debarati Chatterjee,[11] Deep Chatterjee,[6] M. Chaturvedi,[94] S. Chaty,[45] C. Chen,[133,134] D. Chen,[52] H. Y. Chen,[74] J. Chen,[129] K. Chen,[135] X. Chen,[93] Y.-B. Chen,[136] Y.-R. Chen,[137] Z. Chen,[17] H. Cheng,[76] C. K. Cheong,[130] H. Y. Cheung,[130] H. Y. Chia,[76] F. Chiadini,[138,103] C-Y. Chiang,[139] G. Chiarini,[81] R. Chierici,[140] A. Chincarini,[92] M. L. Chiofalo,[78,18] A. Chiummo,[47] R. K. Choudhary,[93] S. Choudhary,[11] N. Christensen,[37] Q. Chu,[93] Y-K. Chu,[139] S. S. Y. Chua,[8] K. W. Chung,[60] G. Ciani,[80,81] P. Ciecielag,[86] M. Cieślar,[86] M. Cifaldi,[123,124] A. A. Ciobanu,[88] R. Ciolfi,[141,81] F. Cipriano,[37] F. Clara,[72] J. A. Clark,[1,48] P. Clearwater,[142] S. Clesse,[143] F. Cleva,[37] E. Coccia,[32,107] E. Codazzo,[32] P.-F. Cohadon,[108] D. E. Cohen,[46] M. Colleoni,[144] C. G. Collette,[145] A. Colombo,[69,70] M. Colpi,[69,70] C. M. Compton,[72] M. Constancio Jr.,[16] L. Conti,[81] S. J. Cooper,[14] P. Corban,[56] T. R. Corbitt,[7] I. Cordero-Carrión,[146] S. Corezzi,[79,40] K. R. Corley,[50] N. J. Cornish,[83] D. Corre,[46] A. Corsi,[147] S. Cortese,[47] C. A. Costa,[16] R. Cotesta,[111] R. Cottingham,[56] M. W. Coughlin,[148] J.-P. Coulon,[37] S. T. Countryman,[50] B. Cousins,[149] P. Couvares,[1] D. M. Coward,[93] M. J. Cowart,[56] D. C. Coyne,[1] R. Coyne,[150] J. D. E. Creighton,[6] T. D. Creighton,[89] A. W. Criswell,[148] M. Croquette,[108] S. G. Crowder,[151] J. R. Cudell,[68] T. J. Cullen,[7] A. Cumming,[24] R. Cummings,[24] L. Cunningham,[24] E. Cuoco,[47,152,18] M. Curyło,[109] P. Dabadie,[26]

T. Dal Canton,[46] S. Dall'Osso,[32] G. Dálya,[85,153] A. Dana,[77] B. D'Angelo,[118,92] S. Danilishin,[154,59] S. D'Antonio,[124] K. Danzmann,[9,10] C. Darsow-Fromm,[127] A. Dasgupta,[84] L. E. H. Datrier,[24] Sayak Datta,[11] Sayantani Datta,[155] V. Dattilo,[47] I. Dave,[94] M. Davier,[46] D. Davis,[1] M. C. Davis,[113] E. J. Daw,[156] R. Dean,[113] D. DeBra,[77] M. Deenadayalan,[11] J. Degallaix,[157] M. De Laurentis,[25,4] S. Deléglise,[108] V. Del Favero,[128] F. De Lillo,[58] N. De Lillo,[24] D. Dell'Aquila,[121] W. Del Pozzo,[78,18] L. M. DeMarchi,[15] F. De Matteis,[123,124] V. D'Emilio,[17] N. Demos,[74] T. Dent,[114] A. Depasse,[58] R. De Pietri,[158,159] R. De Rosa,[25,4] C. De Rossi,[47] R. DeSalvo,[125,160] R. De Simone,[138] S. Dhurandhar,[11] M. C. Díaz,[89] N. A. Didio,[67] T. Dietrich,[111] L. Di Fiore,[4] C. Di Fronzo,[14] C. Di Giorgio,[102,103] F. Di Giovanni,[126] M. Di Giovanni,[32] T. Di Girolamo,[25,4] A. Di Lieto,[78,18] A. Di Michele,[79] B. Ding,[145] S. Di Pace,[104,57] I. Di Palma,[104,57] F. Di Renzo,[78,18] A. K. Divakarla,[76] A. Dmitriev,[14] Z. Doctor,[15] L. Donahue,[161] L. D'Onofrio,[25,4] F. Donovan,[74] K. L. Dooley,[17] S. Doravari,[11] M. Drago,[104,57] J. C. Driggers,[72] Y. Drori,[1] J.-G. Ducoin,[46] P. Dupej,[24] U. Dupletsa,[32] O. Durante,[102,103] D. D'Urso,[121,122] P.-A. Duverne,[46] S. E. Dwyer,[72] C. Eassa,[72] P. J. Easter,[5] M. Ebersold,[162] T. Eckhardt,[127] G. Eddolls,[24] B. Edelman,[66] T. B. Edo,[1] O. Edy,[51] A. Effler,[56] S. Eguchi,[131] J. Eichholz,[8] S. S. Eikenberry,[76] M. Eisenmann,[30,20] R. A. Eisenstein,[74] A. Ejlli,[17] E. Engelby,[44] Y. Enomoto,[27] L. Errico,[25,4] R. C. Essick,[163] H. Estellés,[144] D. Estevez,[164] Z. Etienne,[165] T. Etzel,[1] M. Evans,[74] T. M. Evans,[56] T. Evstafyeva,[12] B. E. Ewing,[149] F. Fabrizi,[54,55] F. Faedi,[55] V. Fafone,[123,124,32] H. Fair,[67] S. Fairhurst,[17] P. C. Fan,[161] A. M. Farah,[166] S. Farinon,[92] B. Farr,[66] W. M. Farr,[115,116] E. J. Fauchon-Jones,[17] G. Favaro,[80] M. Favata,[167] M. Fays,[68] M. Fazio,[168] J. Feicht,[1] M. M. Fejer,[77] E. Fenyvesi,[75,169] D. L. Ferguson,[170] A. Fernandez-Galiana,[74] I. Ferrante,[78,18] T. A. Ferreira,[16] F. Fidecaro,[78,18] P. Figura,[109] A. Fiori,[18,78] I. Fiori,[47] M. Fishbach,[15] R. P. Fisher,[63] R. Fittipaldi,[171,103] V. Fiumara,[172,103] R. Flaminio,[30,20] E. Floden,[148] H. K. Fong,[28] J. A. Font,[126,173] B. Fornal,[160] P. W. F. Forsyth,[8] A. Franke,[127] S. Frasca,[104,57] F. Frasconi,[18] J. P. Freed,[36] Z. Frei,[153] A. Freise,[59,96] O. Freitas,[174] R. Frey,[66] P. Fritschel,[74] V. V. Frolov,[56] G. G. Fronzé,[23] Y. Fujii,[175] Y. Fujikawa,[176] Y. Fujimoto,[177] P. Fulda,[76] M. Fyffe,[56] H. A. Gabbard,[24] B. U. Gadre,[111] J. R. Gair,[111] J. Gais,[130] S. Galaudage,[5] R. Gamba,[13] D. Ganapathy,[74] A. Ganguly,[11] D. Gao,[178] S. G. Gaonkar,[11] B. Garaventa,[92,118] C. García Núñez,[100] C. García-Quirós,[144] F. Garufi,[25,4] B. Gateley,[72] V. Gayathri,[76] G.-G. Ge,[178] G. Gemme,[92] A. Gennai,[18] J. George,[94] O. Gerberding,[127] L. Gergely,[179] P. Gewecke,[127] S. Ghonge,[48] Abhirup Ghosh,[111] Archisman Ghosh,[85] Shaon Ghosh,[167] Shrobana Ghosh,[17] Tathagata Ghosh,[11] B. Giacomazzo,[69,70,71] L. Giacoppo,[104,57] J. A. Giaime,[7,56] K. D. Giardina,[56] D. R. Gibson,[100] C. Gier,[33] M. Giesler,[180] P. Giri,[18,78] F. Gissi,[87] S. Gkaitatzis,[18,78] J. Glanzer,[7] A. E. Gleckl,[44] P. Godwin,[149] E. Goetz,[181] R. Goetz,[76] N. Gohlke,[9,10] J. Golomb,[1] B. Goncharov,[32] G. González,[7] M. Gosselin,[47] R. Gouaty,[30] D. W. Gould,[8] S. Goyal,[19] B. Grace,[8] A. Grado,[182,4] V. Graham,[24] M. Granata,[157] V. Granata,[102] A. Grant,[24] S. Gras,[74] P. Grassia,[1] C. Gray,[72] R. Gray,[24] G. Greco,[40] A. C. Green,[76] R. Green,[17] A. M. Gretarsson,[36] E. M. Gretarsson,[36] D. Griffith,[1] W. L. Griffiths,[17] H. L. Griggs,[48] G. Grignani,[79,40] A. Grimaldi,[98,99] E. Grimes,[36] S. J. Grimm,[32,107] H. Grote,[17] S. Grunewald,[111] P. Gruning,[46] A. S. Gruson,[44] D. Guerra,[126] G. M. Guidi,[54,55] A. R. Guimaraes,[7] G. Guixé,[29] H. K. Gulati,[84] A. M. Gunny,[74] H.-K. Guo,[160] Y. Guo,[59] Anchal Gupta,[1] Anuradha Gupta,[183] I. M. Gupta,[149] P. Gupta,[59,65] S. K. Gupta,[106] R. Gustafson,[184] F. Guzman,[185] S. Ha,[186] I. P. W. Hadiputrawan,[135] L. Haegel,[45] S. Haino,[139] O. Halim,[35] E. D. Hall,[74] E. Z. Hamilton,[162] G. Hammond,[24] W.-B. Han,[187] M. Haney,[162] J. Hanks,[72] C. Hanna,[149] M. D. Hannam,[17] O. Hannuksela,[65,59] H. Hansen,[72] T. J. Hansen,[36] J. Hanson,[56] T. Harder,[37] K. Haris,[59,65] J. Harms,[32,107] G. M. Harry,[42] I. W. Harry,[51] D. Hartwig,[127] K. Hasegawa,[188] B. Haskell,[86] C.-J. Haster,[74] J. S. Hathaway,[128] K. Hattori,[189] K. Haughian,[24] H. Hayakawa,[190] K. Hayama,[131] F. J. Hayes,[24] J. Healy,[128] A. Heidmann,[108] A. Heidt,[9,10] M. C. Heintze,[56] J. Heinze,[9,10] J. Heinzel,[74] H. Heitmann,[37] F. Hellman,[191] P. Hello,[46] A. F. Helmling-Cornell,[66] G. Hemming,[47] M. Hendry,[24] I. S. Heng,[24] E. Hennes,[59] J. Hennig,[192] M. H. Hennig,[192] C. Henshaw,[48] A. G. Hernandez,[90] F. Hernandez Vivanco,[5] M. Heurs,[9,10] A. L. Hewitt,[193] S. Higginbotham,[17] S. Hild,[154,59] P. Hill,[33] Y. Himemoto,[194] A. S. Hines,[185] N. Hirata,[20] C. Hirose,[176] T-C. Ho,[135] S. Hochheim,[9,10] D. Hofman,[157] J. N. Hohmann,[127] D. G. Holcomb,[113] N. A. Holland,[8] I. J. Hollows,[156] Z. J. Holmes,[88] K. Holt,[56] D. E. Holz,[166] Q. Hong,[129] J. Hough,[24] S. Hourihane,[1] E. J. Howell,[93] C. G. Hoy,[17] D. Hoyland,[14] A. Hreibi,[9,10] B-H. Hsieh,[188] H-F. Hsieh,[195] C. Hsiung,[133] Y. Hsu,[129] H-Y. Huang,[139] P. Huang,[178] Y-C. Huang,[137] Y.-J. Huang,[139] Yiting Huang,[151] Yiwen Huang,[74] M. T. Hübner,[5] A. D. Huddart,[196] B. Hughey,[36] D. C. Y. Hui,[197] V. Hui,[30] S. Husa,[144] S. H. Huttner,[24] R. Huxford,[149] T. Huynh-Dinh,[56] S. Ide,[198] B. Idzkowski,[109] A. Iess,[123,124] K. Inayoshi,[199] Y. Inoue,[135] P. Iosif,[200] M. Isi,[74] K. Isleif,[127] K. Ito,[201] Y. Itoh,[177,202] B. R. Iyer,[19]

V. JaberianHamedan,[93] T. Jacqmin,[108] P.-E. Jacquet,[108] S. J. Jadhav,[203] S. P. Jadhav,[11] T. Jain,[12] A. L. James,[17] A. Z. Jan,[170] K. Jani,[204] J. Janquart,[65,59] K. Janssens,[205,37] N. N. Janthalur,[203] P. Jaranowski,[206] D. Jariwala,[76] R. Jaume,[144] A. C. Jenkins,[60] K. Jenner,[88] C. Jeon,[207] W. Jia,[74] J. Jiang,[76] H.-B. Jin,[208,209] G. R. Johns,[63] R. Johnston,[24] A. W. Jones,[93] D. I. Jones,[210] P. Jones,[14] R. Jones,[24] P. Joshi,[149] L. Ju,[93] A. Jue,[160] P. Jung,[62] K. Jung,[186] J. Junker,[9,10] V. Juste,[164] K. Kaihotsu,[201] T. Kajita,[211] M. Kakizaki,[189] C. V. Kalaghatgi,[17,65,59,212] V. Kalogera,[15] B. Kamai,[1] M. Kamiizumi,[190] N. Kanda,[177,202] S. Kandhasamy,[11] G. Kang,[213] J. B. Kanner,[1] Y. Kao,[129] S. J. Kapadia,[19] D. P. Kapasi,[8] C. Karathanasis,[31] S. Karki,[95] R. Kashyap,[149] M. Kasprzack,[1] W. Kastaun,[9,10] T. Kato,[188] S. Katsanevas,[47] E. Katsavounidis,[74] W. Katzman,[56] T. Kaur,[93] K. Kawabe,[72] K. Kawaguchi,[188] F. Kéfélian,[37] D. Keitel,[144] J. S. Key,[214] S. Khadka,[77] F. Y. Khalili,[97] S. Khan,[17] T. Khanam,[147] E. A. Khazanov,[215] N. Khetan,[32,107] M. Khursheed,[94] N. Kijbunchoo,[8] A. Kim,[15] C. Kim,[207] J. C. Kim,[216] J. Kim,[217] K. Kim,[207] W. S. Kim,[62] Y.-M. Kim,[186] C. Kimball,[15] N. Kimura,[190] M. Kinley-Hanlon,[24] R. Kirchhoff,[9,10] J. S. Kissel,[72] S. Klimenko,[76] T. Klinger,[12] A. M. Knee,[181] T. D. Knowles,[165] N. Knust,[9,10] E. Knyazev,[74] Y. Kobayashi,[177] P. Koch,[9,10] G. Koekoek,[59,154] K. Kohri,[218] K. Kokeyama,[219] S. Koley,[32] P. Kolitsidou,[17] M. Kolstein,[31] K. Komori,[74] V. Kondrashov,[1] A. K. H. Kong,[195] A. Kontos,[82] N. Koper,[9,10] M. Korobko,[127] M. Kovalam,[93] N. Koyama,[176] D. B. Kozak,[1] C. Kozakai,[52] V. Kringel,[9,10] N. V. Krishnendu,[9,10] A. Królak,[220,221] G. Kuehn,[9,10] F. Kuei,[129] P. Kuijer,[59] S. Kulkarni,[183] A. Kumar,[203] Prayush Kumar,[19] Rahul Kumar,[72] Rakesh Kumar,[84] J. Kume,[28] K. Kuns,[74] Y. Kuromiya,[201] S. Kuroyanagi,[222,223] K. Kwak,[186] G. Lacaille,[24] P. Lagabbe,[30] D. Laghi,[112] E. Lalande,[224] M. Lalleman,[205] T. L. Lam,[130] A. Lamberts,[37,225] M. Landry,[72] B. B. Lane,[74] R. N. Lang,[74] J. Lange,[170] B. Lantz,[77] I. La Rosa,[30] A. Lartaux-Vollard,[46] P. D. Lasky,[5] M. Laxen,[56] A. Lazzarini,[1] C. Lazzaro,[80,81] P. Leaci,[104,57] S. Leavey,[9,10] S. LeBohec,[160] Y. K. Lecoeuche,[181] E. Lee,[188] H. M. Lee,[226] H. W. Lee,[216] K. Lee,[227] R. Lee,[137] I. N. Legred,[1] J. Lehmann,[9,10] A. Lemaître,[228] M. Lenti,[55,229] M. Leonardi,[20] E. Leonova,[38] N. Leroy,[46] N. Letendre,[30] C. Levesque,[224] Y. Levin,[5] J. N. Leviton,[184] K. Leyde,[45] A. K. Y. Li,[1] B. Li,[129] J. Li,[15] K. L. Li,[230] P. Li,[231] T. G. F. Li,[130] X. Li,[136] C-Y. Lin,[232] E. T. Lin,[195] F-K. Lin,[139] F-L. Lin,[233] H. L. Lin,[135] L. C.-C. Lin,[230] F. Linde,[212,59] S. D. Linker,[125,90] J. N. Linley,[24] T. B. Littenberg,[234] G. C. Liu,[133] J. Liu,[93] K. Liu,[129] X. Liu,[6] F. Llamas,[89] R. K. L. Lo,[1] T. Lo,[129] L. T. London,[38,74] A. Longo,[235] D. Lopez,[162] M. Lopez Portilla,[65] M. Lorenzini,[123,124] V. Loriette,[236] M. Lormand,[56] G. Losurdo,[18] T. P. Lott,[48] J. D. Lough,[9,10] C. O. Lousto,[128] G. Lovelace,[44] J. F. Lucaccioni,[237] H. Lück,[9,10] D. Lumaca,[123,124] A. P. Lundgren,[51] L.-W. Luo,[139] J. E. Lynam,[63] M. Ma'arif,[135] R. Macas,[51] J. B. Machtinger,[15] M. MacInnis,[74] D. M. Macleod,[17] I. A. O. MacMillan,[1] A. Macquet,[37] I. Magaña Hernandez,[6] C. Magazzù,[18] R. M. Magee,[1] R. Maggiore,[14] M. Magnozzi,[92,118] S. Mahesh,[165] E. Majorana,[104,57] I. Maksimovic,[236] S. Maliakal,[1] A. Malik,[94] N. Man,[37] V. Mandic,[148] V. Mangano,[104,57] G. L. Mansell,[72,74] M. Manske,[6] M. Mantovani,[47] M. Mapelli,[80,81] F. Marchesoni,[41,40,238] D. Marín Pina,[29] F. Marion,[30] Z. Mark,[136] S. Márka,[50] Z. Márka,[50] C. Markakis,[12] A. S. Markosyan,[77] A. Markowitz,[1] E. Maros,[1] A. Marquina,[146] S. Marsat,[45] F. Martelli,[54,55] I. W. Martin,[24] R. M. Martin,[167] M. Martinez,[31] V. A. Martinez,[76] V. Martinez,[26] K. Martinovic,[60] D. V. Martynov,[14] E. J. Marx,[74] H. Masalehdan,[127] K. Mason,[74] E. Massera,[156] A. Masserot,[30] M. Masso-Reid,[24] S. Mastrogiovanni,[45] A. Matas,[111] M. Mateu-Lucena,[144] F. Matichard,[1,74] M. Matiushechkina,[9,10] N. Mavalvala,[74] J. J. McCann,[93] R. McCarthy,[72] D. E. McClelland,[8] P. K. McClincy,[149] S. McCormick,[56] L. McCuller,[74] G. I. McGhee,[24] S. C. McGuire,[56] C. McIsaac,[51] J. McIver,[181] T. McRae,[8] S. T. McWilliams,[165] D. Meacher,[6] M. Mehmet,[9,10] A. K. Mehta,[111] Q. Meijer,[65] A. Melatos,[120] D. A. Melchor,[44] G. Mendell,[72] A. Menendez-Vazquez,[31] C. S. Menoni,[168] R. A. Mercer,[6] L. Mereni,[157] K. Merfeld,[66] E. L. Merilh,[56] J. D. Merritt,[66] M. Merzougui,[37] S. Meshkov,[1,*] C. Messenger,[24] C. Messick,[74] P. M. Meyers,[120] F. Meylahn,[9,10] A. Mhaske,[11] A. Miani,[98,99] H. Miao,[14] I. Michaloliakos,[76] C. Michel,[157] Y. Michimura,[27] H. Middleton,[120] D. P. Mihaylov,[111] L. Milano,[25,†] A. L. Miller,[58] A. Miller,[90] B. Miller,[38,59] M. Millhouse,[120] J. C. Mills,[17] E. Milotti,[239,35] Y. Minenkov,[124] N. Mio,[240] Ll. M. Mir,[31] M. Miravet-Tenés,[126] A. Mishkin,[76] C. Mishra,[241] T. Mishra,[76] T. Mistry,[156] S. Mitra,[11] V. P. Mitrofanov,[97] G. Mitselmakher,[76] R. Mittleman,[74] O. Miyakawa,[190] K. Miyo,[190] S. Miyoki,[190] Geoffrey Mo,[74] L. M. Modafferi,[144] E. Moguel,[237] K. Mogushi,[95] S. R. P. Mohapatra,[74] S. R. Mohite,[6] I. Molina,[44] M. Molina-Ruiz,[191] M. Mondin,[90] M. Montani,[54,55] C. J. Moore,[14] J. Moragues,[144] D. Moraru,[72] F. Morawski,[86] A. More,[11] C. Moreno,[36] G. Moreno,[72] Y. Mori,[201] S. Morisaki,[6] N. Morisue,[177] Y. Moriwaki,[189] B. Mours,[164] C. M. Mow-Lowry,[59,96] S. Mozzon,[51] F. Muciaccia,[104,57] Arunava Mukherjee,[242] D. Mukherjee,[149] Soma Mukherjee,[89] Subroto Mukherjee,[84] Suvodip Mukherjee,[163,38] N. Mukund,[9,10]

A. Mullavey,[56] J. Munch,[88] E. A. Muñiz,[67] P. G. Murray,[24] R. Musenich,[92, 118] S. Muusse,[88] S. L. Nadji,[9, 10] K. Nagano,[243] A. Nagar,[23, 244] K. Nakamura,[20] H. Nakano,[245] M. Nakano,[188] Y. Nakayama,[201] V. Napolano,[47] I. Nardecchia,[123, 124] T. Narikawa,[188] H. Narola,[65] L. Naticchioni,[57] B. Nayak,[90] R. K. Nayak,[246] B. F. Neil,[93] J. Neilson,[87, 103] A. Nelson,[185] T. J. N. Nelson,[56] M. Nery,[9, 10] P. Neubauer,[237] A. Neunzert,[214] K. Y. Ng,[74] S. W. S. Ng,[88] C. Nguyen,[45] P. Nguyen,[66] T. Nguyen,[74] L. Nguyen Quynh,[247] J. Ni,[148] W.-T. Ni,[208, 178, 137] S. A. Nichols,[7] T. Nishimoto,[188] A. Nishizawa,[28] S. Nissanke,[38, 59] E. Nitoglia,[140] F. Nocera,[47] M. Norman,[17] C. North,[17] S. Nozaki,[189] G. Nurbek,[89] L. K. Nuttall,[51] Y. Obayashi,[188] J. Oberling,[72] B. D. O'Brien,[76] J. O'Dell,[196] E. Oelker,[24] W. Ogaki,[188] G. Oganesyan,[32, 107] J. J. Oh,[62] K. Oh,[197] S. H. Oh,[62] M. Ohashi,[190] T. Ohashi,[177] M. Ohkawa,[176] F. Ohme,[9, 10] H. Ohta,[28] M. A. Okada,[16] Y. Okutani,[198] C. Olivetto,[47] K. Oohara,[188, 248] R. Oram,[56] B. O'Reilly,[56] R. G. Ormiston,[148] N. D. Ormsby,[63] R. O'Shaughnessy,[128] E. O'Shea,[180] S. Oshino,[190] S. Ossokine,[111] C. Osthelder,[1] S. Otabe,[2] D. J. Ottaway,[88] H. Overmier,[56] A. E. Pace,[149] G. Pagano,[78, 18] R. Pagano,[7] M. A. Page,[93] G. Pagliaroli,[32, 107] A. Pai,[106] S. A. Pai,[94] S. Pal,[246] J. R. Palamos,[66] O. Palashov,[215] C. Palomba,[57] H. Pan,[129] K.-C. Pan,[137, 195] P. K. Panda,[203] P. T. H. Pang,[59, 65] C. Pankow,[15] F. Pannarale,[104, 57] B. C. Pant,[94] F. H. Panther,[93] F. Paoletti,[18] A. Paoli,[47] A. Paolone,[57, 249] G. Pappas,[200] A. Parisi,[133] H. Park,[6] J. Park,[250] W. Parker,[56] D. Pascucci,[59, 85] A. Pasqualetti,[47] R. Passaquieti,[78, 18] D. Passuello,[18] M. Patel,[63] M. Pathak,[88] B. Patricelli,[47, 18] A. S. Patron,[7] S. Paul,[66] E. Payne,[5] M. Pedraza,[1] R. Pedurand,[103] M. Pegoraro,[81] A. Pele,[56] F. E. Peña Arellano,[190] S. Penano,[77] S. Penn,[251] A. Perego,[98, 99] A. Pereira,[26] T. Pereira,[252] C. J. Perez,[72] C. Périgois,[30] C. C. Perkins,[76] A. Perreca,[98, 99] S. Perriès,[140] D. Pesios,[200] J. Petermann,[127] D. Petterson,[1] H. P. Pfeiffer,[111] H. Pham,[56] K. A. Pham,[148] K. S. Phukon,[59, 212] H. Phurailatpam,[130] O. J. Piccinni,[57] M. Pichot,[37] M. Piendibene,[78, 18] F. Piergiovanni,[54, 55] L. Pierini,[104, 57] V. Pierro,[87, 103] G. Pillant,[47] M. Pillas,[46] F. Pilo,[18] L. Pinard,[157] C. Pineda-Bosque,[90] I. M. Pinto,[87, 103, 253] M. Pinto,[47] B. J. Piotrzkowski,[6] K. Piotrzkowski,[58] M. Pirello,[72] M. D. Pitkin,[193] A. Placidi,[40, 79] E. Placidi,[104, 57] M. L. Planas,[144] W. Plastino,[254, 235] C. Pluchar,[255] R. Poggiani,[78, 18] E. Polini,[30] D. Y. T. Pong,[130] S. Ponrathnam,[11] E. K. Porter,[45] R. Poulton,[47] A. Poverman,[82] J. Powell,[142] M. Pracchia,[30] T. Pradier,[164] A. K. Prajapati,[84] K. Prasai,[77] R. Prasanna,[203] G. Pratten,[14] M. Principe,[87, 253, 103] G. A. Prodi,[256, 99] L. Prokhorov,[14] P. Prosposito,[123, 124] L. Prudenzi,[111] A. Puecher,[59, 65] M. Punturo,[40] F. Puosi,[18, 78] P. Puppo,[57] M. Pürrer,[111] H. Qi,[17] N. Quartey,[63] V. Quetschke,[89] P. J. Quinonez,[36] R. Quitzow-James,[95] F. J. Raab,[72] G. Raaijmakers,[38, 59] H. Radkins,[72] N. Radulesco,[37] P. Raffai,[153] S. X. Rail,[224] S. Raja,[94] C. Rajan,[94] K. E. Ramirez,[56] T. D. Ramirez,[44] A. Ramos-Buades,[111] J. Rana,[149] P. Rapagnani,[104, 57] A. Ray,[6] V. Raymond,[17] N. Raza,[181] M. Razzano,[78, 18] J. Read,[44] L. A. Rees,[42] T. Regimbau,[30] L. Rei,[92] S. Reid,[33] S. W. Reid,[63] D. H. Reitze,[1, 76] P. Relton,[17] A. Renzini,[1] P. Rettegno,[22, 23] B. Revenu,[45] A. Reza,[59] M. Rezac,[44] F. Ricci,[104, 57] D. Richards,[196] J. W. Richardson,[257] L. Richardson,[185] G. Riemenschneider,[22, 23] K. Riles,[184] S. Rinaldi,[78, 18] K. Rink,[181] N. A. Robertson,[1] R. Robie,[1] F. Robinet,[46] A. Rocchi,[124] S. Rodriguez,[44] L. Rolland,[30] J. G. Rollins,[1] M. Romanelli,[105] R. Romano,[3, 4] C. L. Romel,[72] A. Romero,[31] I. M. Romero-Shaw,[5] J. H. Romie,[56] S. Ronchini,[32, 107] L. Rosa,[4, 25] C. A. Rose,[6] D. Rosińska,[109] M. P. Ross,[258] S. Rowan,[24] S. J. Rowlinson,[14] S. Roy,[65] Santosh Roy,[11] Soumen Roy,[259] D. Rozza,[121, 122] P. Ruggi,[47] K. Ruiz-Rocha,[204] K. Ryan,[72] S. Sachdev,[149] T. Sadecki,[72] J. Sadiq,[114] S. Saha,[195] Y. Saito,[190] K. Sakai,[260] M. Sakellariadou,[60] S. Sakon,[149] O. S. Salafia,[71, 70, 69] F. Salces-Carcoba,[1] L. Salconi,[47] M. Saleem,[148] F. Salemi,[98, 99] A. Samajdar,[70] E. J. Sanchez,[1] J. H. Sanchez,[44] L. E. Sanchez,[1] N. Sanchis-Gual,[261] J. R. Sanders,[262] A. Sanuy,[29] T. R. Saravanan,[11] N. Sarin,[5] B. Sassolas,[157] H. Satari,[93] B. S. Sathyaprakash,[149, 17] O. Sauter,[76] R. L. Savage,[72] V. Savant,[11] T. Sawada,[177] H. L. Sawant,[11] S. Sayah,[157] D. Schaetzl,[1] M. Scheel,[136] J. Scheuer,[15] M. G. Schiworski,[88] P. Schmidt,[14] S. Schmidt,[65] R. Schnabel,[127] M. Schneewind,[9, 10] R. M. S. Schofield,[66] A. Schönbeck,[127] B. W. Schulte,[9, 10] B. F. Schutz,[17, 9, 10] E. Schwartz,[17] J. Scott,[24] S. M. Scott,[8] M. Seglar-Arroyo,[30] Y. Sekiguchi,[263] D. Sellers,[56] A. S. Sengupta,[259] D. Sentenac,[47] E. G. Seo,[130] V. Sequino,[25, 4] A. Sergeev,[215] Y. Setyawati,[9, 10, 65] T. Shaffer,[72] M. S. Shahriar,[15] M. A. Shaikh,[19] B. Shams,[160] L. Shao,[199] A. Sharma,[32, 107] P. Sharma,[94] P. Shawhan,[110] N. S. Shcheblanov,[228] A. Sheela,[241] Y. Shikano,[264, 265] M. Shikauchi,[28] H. Shimizu,[266] K. Shimode,[190] H. Shinkai,[267] T. Shishido,[53] A. Shoda,[20] D. H. Shoemaker,[74] D. M. Shoemaker,[170] S. ShyamSundar,[94] M. Sieniawska,[58] D. Sigg,[72] L. Silenzi,[40, 41] L. P. Singer,[117] D. Singh,[149] M. K. Singh,[19] N. Singh,[109] A. Singha,[154, 59] A. M. Sintes,[144] V. Sipala,[121, 122] V. Skliris,[17] B. J. J. Slagmolen,[8] T. J. Slaven-Blair,[93] J. Smetana,[14] J. R. Smith,[44] L. Smith,[24] R. J. E. Smith,[5] J. Soldateschi,[229, 268, 55] S. N. Somala,[269] K. Somiya,[2] I. Song,[195] K. Soni,[11] V. Sordini,[140] F. Sorrentino,[92] N. Sorrentino,[78, 18] R. Soulard,[37]

T. Souradeep,[270,11] E. Sowell,[147] V. Spagnuolo,[154,59] A. P. Spencer,[24] M. Spera,[80,81] P. Spinicelli,[47] A. K. Srivastava,[84] V. Srivastava,[67] K. Staats,[15] C. Stachie,[37] F. Stachurski,[24] D. A. Steer,[45] J. Steinlechner,[154,59] S. Steinlechner,[154,59] N. Stergioulas,[200] D. J. Stops,[14] M. Stover,[237] K. A. Strain,[24] L. C. Strang,[120] G. Stratta,[271,57] M. D. Strong,[7] A. Strunk,[72] R. Sturani,[252] A. L. Stuver,[113] M. Suchenek,[86] S. Sudhagar,[11] V. Sudhir,[74] R. Sugimoto,[272,243] H. G. Suh,[6] A. G. Sullivan,[50] T. Z. Summerscales,[273] L. Sun,[8] S. Sunil,[84] A. Sur,[86] J. Suresh,[28] P. J. Sutton,[17] Takamasa Suzuki,[176] Takanori Suzuki,[2] Toshikazu Suzuki,[188] B. L. Swinkels,[59] M. J. Szczepańczyk,[76] P. Szewczyk,[109] M. Tacca,[59] H. Tagoshi,[188] S. C. Tait,[24] H. Takahashi,[274] R. Takahashi,[20] S. Takano,[27] H. Takeda,[27] M. Takeda,[177] C. J. Talbot,[33] C. Talbot,[1] K. Tanaka,[275] Taiki Tanaka,[188] Takahiro Tanaka,[276] A. J. Tanasijczuk,[58] S. Tanioka,[190] D. B. Tanner,[76] D. Tao,[1] L. Tao,[76] R. D. Tapia,[149] E. N. Tapia San Martín,[59] C. Taranto,[123] A. Taruya,[277] J. D. Tasson,[161] R. Tenorio,[144] J. E. S. Terhune,[113] L. Terkowski,[127] M. P. Thirugnanasambandam,[11] M. Thomas,[56] P. Thomas,[72] E. E. Thompson,[48] J. E. Thompson,[17] S. R. Thondapu,[94] K. A. Thorne,[56] E. Thrane,[5] Shubhanshu Tiwari,[162] Srishti Tiwari,[11] V. Tiwari,[17] A. M. Toivonen,[148] A. E. Tolley,[51] T. Tomaru,[20] T. Tomura,[190] M. Tonelli,[78,18] Z. Tornasi,[24] A. Torres-Forné,[126] C. I. Torrie,[1] I. Tosta e Melo,[122] D. Töyrä,[8] A. Trapananti,[41,40] F. Travasso,[40,41] G. Traylor,[56] M. Trevor,[110] M. C. Tringali,[47] A. Tripathee,[184] L. Troiano,[278,103] A. Trovato,[45] L. Trozzo,[4,190] R. J. Trudeau,[1] D. Tsai,[129] K. W. Tsang,[59,279,65] T. Tsang,[280] J-S. Tsao,[233] M. Tse,[74] R. Tso,[136] S. Tsuchida,[177] L. Tsukada,[149] D. Tsuna,[28] T. Tsutsui,[28] K. Turbang,[281,205] M. Turconi,[37] D. Tuyenbayev,[177] A. S. Ubhi,[14] N. Uchikata,[188] T. Uchiyama,[190] R. P. Udall,[1] A. Ueda,[282] T. Uehara,[283,284] K. Ueno,[28] G. Ueshima,[285] C. S. Unnikrishnan,[286] A. L. Urban,[7] T. Ushiba,[190] A. Utina,[154,59] G. Vajente,[1] A. Vajpeyi,[5] G. Valdes,[185] M. Valentini,[183,98,99] V. Valsan,[6] N. van Bakel,[59] M. van Beuzekom,[59] M. van Dael,[59,287] J. F. J. van den Brand,[154,96,59] C. Van Den Broeck,[65,59] D. C. Vander-Hyde,[67] H. van Haevermaet,[205] J. V. van Heijningen,[58] M. H. P. M. van Putten,[288] N. van Remortel,[205] M. Vardaro,[212,59] A. F. Vargas,[120] V. Varma,[111] M. Vasúth,[75] A. Vecchio,[14] G. Vedovato,[81] J. Veitch,[24] P. J. Veitch,[88] J. Venneberg,[9,10] G. Venugopalan,[1] D. Verkindt,[30] P. Verma,[221] Y. Verma,[94] S. M. Vermeulen,[17] D. Veske,[50] F. Vetrano,[54] A. Viceré,[54,55] S. Vidyant,[67] A. D. Viets,[289] A. Vijaykumar,[19] V. Villa-Ortega,[114] J.-Y. Vinet,[37] A. Virtuoso,[239,35] S. Vitale,[74] H. Vocca,[79,40] E. R. G. von Reis,[72] J. S. A. von Wrangel,[9,10] C. Vorvick,[72] S. P. Vyatchanin,[97] L. E. Wade,[237] M. Wade,[237] K. J. Wagner,[128] R. C. Walet,[59] M. Walker,[63] G. S. Wallace,[33] L. Wallace,[1] J. Wang,[178] J. Z. Wang,[184] W. H. Wang,[89] R. L. Ward,[8] J. Warner,[72] M. Was,[30] T. Washimi,[20] N. Y. Washington,[1] J. Watchi,[145] B. Weaver,[72] C. R. Weaving,[51] S. A. Webster,[24] M. Weinert,[9,10] A. J. Weinstein,[1] R. Weiss,[74] C. M. Weller,[258] R. A. Weller,[204] F. Wellmann,[9,10] L. Wen,[93] P. Weßels,[9,10] K. Wette,[8] J. T. Whelan,[128] D. D. White,[44] B. F. Whiting,[76] C. Whittle,[74] D. Wilken,[9,10] D. Williams,[24] M. J. Williams,[24] A. R. Williamson,[51] J. L. Willis,[1] B. Willke,[9,10] D. J. Wilson,[255] C. C. Wipf,[1] T. Wlodarczyk,[111] G. Woan,[24] J. Woehler,[9,10] J. K. Wofford,[128] D. Wong,[181] I. C. F. Wong,[130] M. Wright,[24] C. Wu,[137] D. S. Wu,[9,10] H. Wu,[137] D. M. Wysocki,[6] L. Xiao,[1] T. Yamada,[266] H. Yamamoto,[1] K. Yamamoto,[189] T. Yamamoto,[190] K. Yamashita,[201] R. Yamazaki,[198] F. W. Yang,[160] K. Z. Yang,[148] L. Yang,[168] Y.-C. Yang,[129] Y. Yang,[290] Yang Yang,[76] M. J. Yap,[8] D. W. Yeeles,[17] S.-W. Yeh,[137] A. B. Yelikar,[128] M. Ying,[129] J. Yokoyama,[28,27] T. Yokozawa,[190] J. Yoo,[180] T. Yoshioka,[201] Hang Yu,[136] Haocun Yu,[74] H. Yuzurihara,[188] A. Zadrożny,[221] M. Zanolin,[36] S. Zeidler,[291] T. Zelenova,[47] J.-P. Zendri,[81] M. Zevin,[166] M. Zhan,[178] H. Zhang,[233] J. Zhang,[93] L. Zhang,[1] R. Zhang,[76] T. Zhang,[14] Y. Zhang,[185] C. Zhao,[93] G. Zhao,[145] Y. Zhao,[188,20] Yue Zhao,[160] R. Zhou,[191] Z. Zhou,[15] X. J. Zhu,[5] Z.-H. Zhu,[119,231] A. B. Zimmerman,[170] M. E. Zucker,[1,74] and J. Zweizig[1]

[1] *LIGO Laboratory, California Institute of Technology, Pasadena, CA 91125, USA*
[2] *Graduate School of Science, Tokyo Institute of Technology, Meguro-ku, Tokyo 152-8551, Japan*
[3] *Dipartimento di Farmacia, Università di Salerno, I-84084 Fisciano, Salerno, Italy*
[4] *INFN, Sezione di Napoli, Complesso Universitario di Monte S. Angelo, I-80126 Napoli, Italy*
[5] *OzGrav, School of Physics & Astronomy, Monash University, Clayton 3800, Victoria, Australia*
[6] *University of Wisconsin-Milwaukee, Milwaukee, WI 53201, USA*
[7] *Louisiana State University, Baton Rouge, LA 70803, USA*
[8] *OzGrav, Australian National University, Canberra, Australian Capital Territory 0200, Australia*
[9] *Max Planck Institute for Gravitational Physics (Albert Einstein Institute), D-30167 Hannover, Germany*
[10] *Leibniz Universität Hannover, D-30167 Hannover, Germany*
[11] *Inter-University Centre for Astronomy and Astrophysics, Pune 411007, India*
[12] *University of Cambridge, Cambridge CB2 1TN, United Kingdom*
[13] *Theoretisch-Physikalisches Institut, Friedrich-Schiller-Universität Jena, D-07743 Jena, Germany*
[14] *University of Birmingham, Birmingham B15 2TT, United Kingdom*
[15] *Northwestern University, Evanston, IL 60208, USA*

[16] *Instituto Nacional de Pesquisas Espaciais, 12227-010 São José dos Campos, São Paulo, Brazil*
[17] *Cardiff University, Cardiff CF24 3AA, United Kingdom*
[18] *INFN, Sezione di Pisa, I-56127 Pisa, Italy*
[19] *International Centre for Theoretical Sciences, Tata Institute of Fundamental Research, Bengaluru 560089, India*
[20] *Gravitational Wave Science Project, National Astronomical Observatory of Japan (NAOJ), Mitaka City, Tokyo 181-8588, Japan*
[21] *Advanced Technology Center, National Astronomical Observatory of Japan (NAOJ), Mitaka City, Tokyo 181-8588, Japan*
[22] *Dipartimento di Fisica, Università degli Studi di Torino, I-10125 Torino, Italy*
[23] *INFN Sezione di Torino, I-10125 Torino, Italy*
[24] *SUPA, University of Glasgow, Glasgow G12 8QQ, United Kingdom*
[25] *Università di Napoli "Federico II", Complesso Universitario di Monte S. Angelo, I-80126 Napoli, Italy*
[26] *Université de Lyon, Université Claude Bernard Lyon 1, CNRS, Institut Lumière Matière, F-69622 Villeurbanne, France*
[27] *Department of Physics, The University of Tokyo, Bunkyo-ku, Tokyo 113-0033, Japan*
[28] *Research Center for the Early Universe (RESCEU), The University of Tokyo, Bunkyo-ku, Tokyo 113-0033, Japan*
[29] *Institut de Ciències del Cosmos (ICCUB), Universitat de Barcelona, C/ Martí i Franquès 1, Barcelona, 08028, Spain*
[30] *Univ. Savoie Mont Blanc, CNRS, Laboratoire d'Annecy de Physique des Particules - IN2P3, F-74000 Annecy, France*
[31] *Institut de Física d'Altes Energies (IFAE), Barcelona Institute of Science and Technology, and ICREA, E-08193 Barcelona, Spain*
[32] *Gran Sasso Science Institute (GSSI), I-67100 L'Aquila, Italy*
[33] *SUPA, University of Strathclyde, Glasgow G1 1XQ, United Kingdom*
[34] *Dipartimento di Scienze Matematiche, Informatiche e Fisiche, Università di Udine, I-33100 Udine, Italy*
[35] *INFN, Sezione di Trieste, I-34127 Trieste, Italy*
[36] *Embry-Riddle Aeronautical University, Prescott, AZ 86301, USA*
[37] *Artemis, Université Côte d'Azur, Observatoire de la Côte d'Azur, CNRS, F-06304 Nice, France*
[38] *GRAPPA, Anton Pannekoek Institute for Astronomy and Institute for High-Energy Physics, University of Amsterdam, Science Park 904, 1098 XH Amsterdam, Netherlands*
[39] *National and Kapodistrian University of Athens, School of Science Building, 2nd floor, Panepistimiopolis, 15771 Ilissia, Greece*
[40] *INFN, Sezione di Perugia, I-06123 Perugia, Italy*
[41] *Università di Camerino, Dipartimento di Fisica, I-62032 Camerino, Italy*
[42] *American University, Washington, D.C. 20016, USA*
[43] *Earthquake Research Institute, The University of Tokyo, Bunkyo-ku, Tokyo 113-0032, Japan*
[44] *California State University Fullerton, Fullerton, CA 92831, USA*
[45] *Université de Paris, CNRS, Astroparticule et Cosmologie, F-75006 Paris, France*
[46] *Université Paris-Saclay, CNRS/IN2P3, IJCLab, 91405 Orsay, France*
[47] *European Gravitational Observatory (EGO), I-56021 Cascina, Pisa, Italy*
[48] *Georgia Institute of Technology, Atlanta, GA 30332, USA*
[49] *Department of Mathematics and Physics,*
[50] *Columbia University, New York, NY 10027, USA*
[51] *University of Portsmouth, Portsmouth, PO1 3FX, United Kingdom*
[52] *Kamioka Branch, National Astronomical Observatory of Japan (NAOJ), Kamioka-cho, Hida City, Gifu 506-1205, Japan*
[53] *The Graduate University for Advanced Studies (SOKENDAI), Mitaka City, Tokyo 181-8588, Japan*
[54] *Università degli Studi di Urbino "Carlo Bo", I-61029 Urbino, Italy*
[55] *INFN, Sezione di Firenze, I-50019 Sesto Fiorentino, Firenze, Italy*
[56] *LIGO Livingston Observatory, Livingston, LA 70754, USA*
[57] *INFN, Sezione di Roma, I-00185 Roma, Italy*
[58] *Université catholique de Louvain, B-1348 Louvain-la-Neuve, Belgium*
[59] *Nikhef, Science Park 105, 1098 XG Amsterdam, Netherlands*
[60] *King's College London, University of London, London WC2R 2LS, United Kingdom*
[61] *Korea Institute of Science and Technology Information, Daejeon 34141, Republic of Korea*
[62] *National Institute for Mathematical Sciences, Daejeon 34047, Republic of Korea*
[63] *Christopher Newport University, Newport News, VA 23606, USA*
[64] *School of High Energy Accelerator Science, The Graduate University for Advanced Studies (SOKENDAI), Tsukuba City, Ibaraki 305-0801, Japan*
[65] *Institute for Gravitational and Subatomic Physics (GRASP), Utrecht University, Princetonplein 1, 3584 CC Utrecht, Netherlands*
[66] *University of Oregon, Eugene, OR 97403, USA*
[67] *Syracuse University, Syracuse, NY 13244, USA*
[68] *Université de Liège, B-4000 Liège, Belgium*
[69] *Università degli Studi di Milano-Bicocca, I-20126 Milano, Italy*
[70] *INFN, Sezione di Milano-Bicocca, I-20126 Milano, Italy*

[71] *INAF, Osservatorio Astronomico di Brera sede di Merate, I-23807 Merate, Lecco, Italy*
[72] *LIGO Hanford Observatory, Richland, WA 99352, USA*
[73] *Dipartimento di Medicina, Chirurgia e Odontoiatria "Scuola Medica Salernitana", Università di Salerno, I-84081 Baronissi, Salerno, Italy*
[74] *LIGO Laboratory, Massachusetts Institute of Technology, Cambridge, MA 02139, USA*
[75] *Wigner RCP, RMKI, H-1121 Budapest, Konkoly Thege Miklós út 29-33, Hungary*
[76] *University of Florida, Gainesville, FL 32611, USA*
[77] *Stanford University, Stanford, CA 94305, USA*
[78] *Università di Pisa, I-56127 Pisa, Italy*
[79] *Università di Perugia, I-06123 Perugia, Italy*
[80] *Università di Padova, Dipartimento di Fisica e Astronomia, I-35131 Padova, Italy*
[81] *INFN, Sezione di Padova, I-35131 Padova, Italy*
[82] *Bard College, Annandale-On-Hudson, NY 12504, USA*
[83] *Montana State University, Bozeman, MT 59717, USA*
[84] *Institute for Plasma Research, Bhat, Gandhinagar 382428, India*
[85] *Universiteit Gent, B-9000 Gent, Belgium*
[86] *Nicolaus Copernicus Astronomical Center, Polish Academy of Sciences, 00-716, Warsaw, Poland*
[87] *Dipartimento di Ingegneria, Università del Sannio, I-82100 Benevento, Italy*
[88] *OzGrav, University of Adelaide, Adelaide, South Australia 5005, Australia*
[89] *The University of Texas Rio Grande Valley, Brownsville, TX 78520, USA*
[90] *California State University, Los Angeles, Los Angeles, CA 90032, USA*
[91] *Departamento de Matemáticas, Universitat Autònoma de Barcelona, Edificio C Facultad de Ciencias 08193 Bellaterra (Barcelona), Spain*
[92] *INFN, Sezione di Genova, I-16146 Genova, Italy*
[93] *OzGrav, University of Western Australia, Crawley, Western Australia 6009, Australia*
[94] *RRCAT, Indore, Madhya Pradesh 452013, India*
[95] *Missouri University of Science and Technology, Rolla, MO 65409, USA*
[96] *Vrije Universiteit Amsterdam, 1081 HV Amsterdam, Netherlands*
[97] *Lomonosov Moscow State University, Moscow 119991, Russia*
[98] *Università di Trento, Dipartimento di Fisica, I-38123 Povo, Trento, Italy*
[99] *INFN, Trento Institute for Fundamental Physics and Applications, I-38123 Povo, Trento, Italy*
[100] *SUPA, University of the West of Scotland, Paisley PA1 2BE, United Kingdom*
[101] *Bar-Ilan University, Ramat Gan, 5290002, Israel*
[102] *Dipartimento di Fisica "E.R. Caianiello", Università di Salerno, I-84084 Fisciano, Salerno, Italy*
[103] *INFN, Sezione di Napoli, Gruppo Collegato di Salerno, Complesso Universitario di Monte S. Angelo, I-80126 Napoli, Italy*
[104] *Università di Roma "La Sapienza", I-00185 Roma, Italy*
[105] *Univ Rennes, CNRS, Institut FOTON - UMR6082, F-3500 Rennes, France*
[106] *Indian Institute of Technology Bombay, Powai, Mumbai 400 076, India*
[107] *INFN, Laboratori Nazionali del Gran Sasso, I-67100 Assergi, Italy*
[108] *Laboratoire Kastler Brossel, Sorbonne Université, CNRS, ENS-Université PSL, Collège de France, F-75005 Paris, France*
[109] *Astronomical Observatory Warsaw University, 00-478 Warsaw, Poland*
[110] *University of Maryland, College Park, MD 20742, USA*
[111] *Max Planck Institute for Gravitational Physics (Albert Einstein Institute), D-14476 Potsdam, Germany*
[112] *L2IT, Laboratoire des 2 Infinis - Toulouse, Université de Toulouse, CNRS/IN2P3, UPS, F-31062 Toulouse Cedex 9, France*
[113] *Villanova University, Villanova, PA 19085, USA*
[114] *IGFAE, Universidade de Santiago de Compostela, 15782 Spain*
[115] *Stony Brook University, Stony Brook, NY 11794, USA*
[116] *Center for Computational Astrophysics, Flatiron Institute, New York, NY 10010, USA*
[117] *NASA Goddard Space Flight Center, Greenbelt, MD 20771, USA*
[118] *Dipartimento di Fisica, Università degli Studi di Genova, I-16146 Genova, Italy*
[119] *Department of Astronomy, Beijing Normal University, Beijing 100875, China*
[120] *OzGrav, University of Melbourne, Parkville, Victoria 3010, Australia*
[121] *Università degli Studi di Sassari, I-07100 Sassari, Italy*
[122] *INFN, Laboratori Nazionali del Sud, I-95125 Catania, Italy*
[123] *Università di Roma Tor Vergata, I-00133 Roma, Italy*
[124] *INFN, Sezione di Roma Tor Vergata, I-00133 Roma, Italy*
[125] *University of Sannio at Benevento, I-82100 Benevento, Italy and INFN, Sezione di Napoli, I-80100 Napoli, Italy*
[126] *Departamento de Astronomía y Astrofísica, Universitat de València, E-46100 Burjassot, València, Spain*
[127] *Universität Hamburg, D-22761 Hamburg, Germany*
[128] *Rochester Institute of Technology, Rochester, NY 14623, USA*

[129] National Tsing Hua University, Hsinchu City, 30013 Taiwan, Republic of China
[130] The Chinese University of Hong Kong, Shatin, NT, Hong Kong
[131] Department of Applied Physics, Fukuoka University, Jonan, Fukuoka City, Fukuoka 814-0180, Japan
[132] OzGrav, Charles Sturt University, Wagga Wagga, New South Wales 2678, Australia
[133] Department of Physics, Tamkang University, Danshui Dist., New Taipei City 25137, Taiwan
[134] Department of Physics and Institute of Astronomy,
National Tsing Hua University, Hsinchu 30013, Taiwan
[135] Department of Physics, Center for High Energy and High Field Physics,
National Central University, Zhongli District, Taoyuan City 32001, Taiwan
[136] CaRT, California Institute of Technology, Pasadena, CA 91125, USA
[137] Department of Physics, National Tsing Hua University, Hsinchu 30013, Taiwan
[138] Dipartimento di Ingegneria Industriale (DIIN),
Università di Salerno, I-84084 Fisciano, Salerno, Italy
[139] Institute of Physics, Academia Sinica, Nankang, Taipei 11529, Taiwan
[140] Université Lyon, Université Claude Bernard Lyon 1, CNRS,
IP2I Lyon / IN2P3, UMR 5822, F-69622 Villeurbanne, France
[141] INAF, Osservatorio Astronomico di Padova, I-35122 Padova, Italy
[142] OzGrav, Swinburne University of Technology, Hawthorn VIC 3122, Australia
[143] Université libre de Bruxelles, Avenue Franklin Roosevelt 50 - 1050 Bruxelles, Belgium
[144] IAC3–IEEC, Universitat de les Illes Balears, E-07122 Palma de Mallorca, Spain
[145] Université Libre de Bruxelles, Brussels 1050, Belgium
[146] Departamento de Matemáticas, Universitat de València, E-46100 Burjassot, València, Spain
[147] Texas Tech University, Lubbock, TX 79409, USA
[148] University of Minnesota, Minneapolis, MN 55455, USA
[149] The Pennsylvania State University, University Park, PA 16802, USA
[150] University of Rhode Island, Kingston, RI 02881, USA
[151] Bellevue College, Bellevue, WA 98007, USA
[152] Scuola Normale Superiore, Piazza dei Cavalieri, 7 - 56126 Pisa, Italy
[153] Eötvös University, Budapest 1117, Hungary
[154] Maastricht University, P.O. Box 616, 6200 MD Maastricht, Netherlands
[155] Chennai Mathematical Institute, Chennai 603103, India
[156] The University of Sheffield, Sheffield S10 2TN, United Kingdom
[157] Université Lyon, Université Claude Bernard Lyon 1,
CNRS, Laboratoire des Matériaux Avancés (LMA),
IP2I Lyon / IN2P3, UMR 5822, F-69622 Villeurbanne, France
[158] Dipartimento di Scienze Matematiche, Fisiche e Informatiche, Università di Parma, I-43124 Parma, Italy
[159] INFN, Sezione di Milano Bicocca, Gruppo Collegato di Parma, I-43124 Parma, Italy
[160] The University of Utah, Salt Lake City, UT 84112, USA
[161] Carleton College, Northfield, MN 55057, USA
[162] University of Zurich, Winterthurerstrasse 190, 8057 Zurich, Switzerland
[163] Perimeter Institute, Waterloo, ON N2L 2Y5, Canada
[164] Université de Strasbourg, CNRS, IPHC UMR 7178, F-67000 Strasbourg, France
[165] West Virginia University, Morgantown, WV 26506, USA
[166] University of Chicago, Chicago, IL 60637, USA
[167] Montclair State University, Montclair, NJ 07043, USA
[168] Colorado State University, Fort Collins, CO 80523, USA
[169] Institute for Nuclear Research, Bem t'er 18/c, H-4026 Debrecen, Hungary
[170] University of Texas, Austin, TX 78712, USA
[171] CNR-SPIN, c/o Università di Salerno, I-84084 Fisciano, Salerno, Italy
[172] Scuola di Ingegneria, Università della Basilicata, I-85100 Potenza, Italy
[173] Observatori Astronòmic, Universitat de València, E-46980 Paterna, València, Spain
[174] Centro de Física das Universidades do Minho e do Porto,
Universidade do Minho, Campus de Gualtar, PT-4710 - 057 Braga, Portugal
[175] Department of Astronomy, The University of Tokyo, Mitaka City, Tokyo 181-8588, Japan
[176] Faculty of Engineering, Niigata University, Nishi-ku, Niigata City, Niigata 950-2181, Japan
[177] Department of Physics, Graduate School of Science,
Osaka City University, Sumiyoshi-ku, Osaka City, Osaka 558-8585, Japan
[178] State Key Laboratory of Magnetic Resonance and Atomic and Molecular Physics,
Innovation Academy for Precision Measurement Science and Technology (APM),
Chinese Academy of Sciences, Xiao Hong Shan, Wuhan 430071, China
[179] University of Szeged, Dóm tér 9, Szeged 6720, Hungary
[180] Cornell University, Ithaca, NY 14850, USA
[181] University of British Columbia, Vancouver, BC V6T 1Z4, Canada
[182] INAF, Osservatorio Astronomico di Capodimonte, I-80131 Napoli, Italy

[183] *The University of Mississippi, University, MS 38677, USA*
[184] *University of Michigan, Ann Arbor, MI 48109, USA*
[185] *Texas A&M University, College Station, TX 77843, USA*
[186] *Ulsan National Institute of Science and Technology, Ulsan 44919, Republic of Korea*
[187] *Shanghai Astronomical Observatory, Chinese Academy of Sciences, Shanghai 200030, China*
[188] *Institute for Cosmic Ray Research (ICRR), KAGRA Observatory, The University of Tokyo, Kashiwa City, Chiba 277-8582, Japan*
[189] *Faculty of Science, University of Toyama, Toyama City, Toyama 930-8555, Japan*
[190] *Institute for Cosmic Ray Research (ICRR), KAGRA Observatory, The University of Tokyo, Kamioka-cho, Hida City, Gifu 506-1205, Japan*
[191] *University of California, Berkeley, CA 94720, USA*
[192] *Maastricht University, 6200 MD, Maastricht, Netherlands*
[193] *Lancaster University, Lancaster LA1 4YW, United Kingdom*
[194] *College of Industrial Technology, Nihon University, Narashino City, Chiba 275-8575, Japan*
[195] *Institute of Astronomy, National Tsing Hua University, Hsinchu 30013, Taiwan*
[196] *Rutherford Appleton Laboratory, Didcot OX11 0DE, United Kingdom*
[197] *Department of Astronomy & Space Science, Chungnam National University, Yuseong-gu, Daejeon 34134, Republic of Korea*
[198] *Department of Physical Sciences, Aoyama Gakuin University, Sagamihara City, Kanagawa 252-5258, Japan*
[199] *Kavli Institute for Astronomy and Astrophysics, Peking University, Haidian District, Beijing 100871, China*
[200] *Aristotle University of Thessaloniki, University Campus, 54124 Thessaloniki, Greece*
[201] *Graduate School of Science and Engineering, University of Toyama, Toyama City, Toyama 930-8555, Japan*
[202] *Nambu Yoichiro Institute of Theoretical and Experimental Physics (NITEP), Osaka City University, Sumiyoshi-ku, Osaka City, Osaka 558-8585, Japan*
[203] *Directorate of Construction, Services & Estate Management, Mumbai 400094, India*
[204] *Vanderbilt University, Nashville, TN 37235, USA*
[205] *Universiteit Antwerpen, Prinsstraat 13, 2000 Antwerpen, Belgium*
[206] *University of Białystok, 15-424 Białystok, Poland*
[207] *Ewha Womans University, Seoul 03760, Republic of Korea*
[208] *National Astronomical Observatories, Chinese Academic of Sciences, Chaoyang District, Beijing, China*
[209] *School of Astronomy and Space Science, University of Chinese Academy of Sciences, Chaoyang District, Beijing, China*
[210] *University of Southampton, Southampton SO17 1BJ, United Kingdom*
[211] *Institute for Cosmic Ray Research (ICRR), The University of Tokyo, Kashiwa City, Chiba 277-8582, Japan*
[212] *Institute for High-Energy Physics, University of Amsterdam, Science Park 904, 1098 XH Amsterdam, Netherlands*
[213] *Chung-Ang University, Seoul 06974, Republic of Korea*
[214] *University of Washington Bothell, Bothell, WA 98011, USA*
[215] *Institute of Applied Physics, Nizhny Novgorod, 603950, Russia*
[216] *Inje University Gimhae, South Gyeongsang 50834, Republic of Korea*
[217] *Department of Physics, Myongji University, Yongin 17058, Republic of Korea*
[218] *Institute of Particle and Nuclear Studies (IPNS), High Energy Accelerator Research Organization (KEK), Tsukuba City, Ibaraki 305-0801, Japan*
[219] *School of Physics and Astronomy, Cardiff University, Cardiff, CF24 3AA, UK*
[220] *Institute of Mathematics, Polish Academy of Sciences, 00656 Warsaw, Poland*
[221] *National Center for Nuclear Research, 05-400 Świerk-Otwock, Poland*
[222] *Instituto de Fisica Teorica, 28049 Madrid, Spain*
[223] *Department of Physics, Nagoya University, Chikusa-ku, Nagoya, Aichi 464-8602, Japan*
[224] *Université de Montréal/Polytechnique, Montreal, Quebec H3T 1J4, Canada*
[225] *Laboratoire Lagrange, Université Côte d'Azur, Observatoire Côte d'Azur, CNRS, F-06304 Nice, France*
[226] *Seoul National University, Seoul 08826, Republic of Korea*
[227] *Sungkyunkwan University, Seoul 03063, Republic of Korea*
[228] *NAVIER, École des Ponts, Univ Gustave Eiffel, CNRS, Marne-la-Vallée, France*
[229] *Università di Firenze, Sesto Fiorentino I-50019, Italy*
[230] *Department of Physics, National Cheng Kung University, Tainan City 701, Taiwan*
[231] *School of Physics and Technology, Wuhan University, Wuhan, Hubei, 430072, China*
[232] *National Center for High-performance computing, National Applied Research Laboratories, Hsinchu Science Park, Hsinchu City 30076, Taiwan*
[233] *Department of Physics, National Taiwan Normal University, sec. 4, Taipei 116, Taiwan*
[234] *NASA Marshall Space Flight Center, Huntsville, AL 35811, USA*
[235] *INFN, Sezione di Roma Tre, I-00146 Roma, Italy*
[236] *ESPCI, CNRS, F-75005 Paris, France*
[237] *Kenyon College, Gambier, OH 43022, USA*
[238] *School of Physics Science and Engineering, Tongji University, Shanghai 200092, China*

[239] *Dipartimento di Fisica, Università di Trieste, I-34127 Trieste, Italy*
[240] *Institute for Photon Science and Technology, The University of Tokyo, Bunkyo-ku, Tokyo 113-8656, Japan*
[241] *Indian Institute of Technology Madras, Chennai 600036, India*
[242] *Saha Institute of Nuclear Physics, Bidhannagar, West Bengal 700064, India*
[243] *Institute of Space and Astronautical Science (JAXA), Chuo-ku, Sagamihara City, Kanagawa 252-0222, Japan*
[244] *Institut des Hautes Etudes Scientifiques, F-91440 Bures-sur-Yvette, France*
[245] *Faculty of Law, Ryukoku University, Fushimi-ku, Kyoto City, Kyoto 612-8577, Japan*
[246] *Indian Institute of Science Education and Research, Kolkata, Mohanpur, West Bengal 741252, India*
[247] *Department of Physics, University of Notre Dame, Notre Dame, IN 46556, USA*
[248] *Graduate School of Science and Technology, Niigata University, Nishi-ku, Niigata City, Niigata 950-2181, Japan*
[249] *Consiglio Nazionale delle Ricerche - Istituto dei Sistemi Complessi, Piazzale Aldo Moro 5, I-00185 Roma, Italy*
[250] *Korea Astronomy and Space Science Institute (KASI), Yuseong-gu, Daejeon 34055, Republic of Korea*
[251] *Hobart and William Smith Colleges, Geneva, NY 14456, USA*
[252] *International Institute of Physics, Universidade Federal do Rio Grande do Norte, Natal RN 59078-970, Brazil*
[253] *Museo Storico della Fisica e Centro Studi e Ricerche "Enrico Fermi", I-00184 Roma, Italy*
[254] *Dipartimento di Matematica e Fisica, Università degli Studi Roma Tre, I-00146 Roma, Italy*
[255] *University of Arizona, Tucson, AZ 85721, USA*
[256] *Università di Trento, Dipartimento di Matematica, I-38123 Povo, Trento, Italy*
[257] *University of California, Riverside, Riverside, CA 92521, USA*
[258] *University of Washington, Seattle, WA 98195, USA*
[259] *Indian Institute of Technology, Palaj, Gandhinagar, Gujarat 382355, India*
[260] *Department of Electronic Control Engineering, National Institute of Technology, Nagaoka College, Nagaoka City, Niigata 940-8532, Japan*
[261] *Departamento de Matemática da Universidade de Aveiro and Centre for Research and Development in Mathematics and Applications, Campus de Santiago, 3810-183 Aveiro, Portugal*
[262] *Marquette University, Milwaukee, WI 53233, USA*
[263] *Faculty of Science, Toho University, Funabashi City, Chiba 274-8510, Japan*
[264] *Graduate School of Science and Technology, Gunma University, Maebashi, Gunma 371-8510, Japan*
[265] *Institute for Quantum Studies, Chapman University, Orange, CA 92866, USA*
[266] *Accelerator Laboratory, High Energy Accelerator Research Organization (KEK), Tsukuba City, Ibaraki 305-0801, Japan*
[267] *Faculty of Information Science and Technology, Osaka Institute of Technology, Hirakata City, Osaka 573-0196, Japan*
[268] *INAF, Osservatorio Astrofisico di Arcetri, Largo E. Fermi 5, I-50125 Firenze, Italy*
[269] *Indian Institute of Technology Hyderabad, Sangareddy, Khandi, Telangana 502285, India*
[270] *Indian Institute of Science Education and Research, Pune, Maharashtra 411008, India*
[271] *Istituto di Astrofisica e Planetologia Spaziali di Roma, Via del Fosso del Cavaliere, 100, 00133 Roma RM, Italy*
[272] *Department of Space and Astronautical Science, The Graduate University for Advanced Studies (SOKENDAI), Sagamihara City, Kanagawa 252-5210, Japan*
[273] *Andrews University, Berrien Springs, MI 49104, USA*
[274] *Research Center for Space Science, Advanced Research Laboratories, Tokyo City University, Setagaya, Tokyo 158-0082, Japan*
[275] *Institute for Cosmic Ray Research (ICRR), Research Center for Cosmic Neutrinos (RCCN), The University of Tokyo, Kashiwa City, Chiba 277-8582, Japan*
[276] *Department of Physics, Kyoto University, Sakyou-ku, Kyoto City, Kyoto 606-8502, Japan*
[277] *Yukawa Institute for Theoretical Physics (YITP), Kyoto University, Sakyou-ku, Kyoto City, Kyoto 606-8502, Japan*
[278] *Dipartimento di Scienze Aziendali - Management and Innovation Systems (DISA-MIS), Università di Salerno, I-84084 Fisciano, Salerno, Italy*
[279] *Van Swinderen Institute for Particle Physics and Gravity, University of Groningen, Nijenborgh 4, 9747 AG Groningen, Netherlands*
[280] *Faculty of Science, Department of Physics, The Chinese University of Hong Kong, Shatin, N.T., Hong Kong*
[281] *Vrije Universiteit Brussel, Pleinlaan 2, 1050 Brussel, Belgium*
[282] *Applied Research Laboratory, High Energy Accelerator Research Organization (KEK), Tsukuba City, Ibaraki 305-0801, Japan*
[283] *Department of Communications Engineering, National Defense Academy of Japan, Yokosuka City, Kanagawa 239-8686, Japan*
[284] *Department of Physics, University of Florida, Gainesville, FL 32611, USA*
[285] *Department of Information and Management Systems Engineering, Nagaoka University of Technology, Nagaoka City, Niigata 940-2188, Japan*
[286] *Tata Institute of Fundamental Research, Mumbai 400005, India*
[287] *Eindhoven University of Technology, Postbus 513, 5600 MB Eindhoven, Netherlands*
[288] *Department of Physics and Astronomy, Sejong University, Gwangjin-gu, Seoul 143-747, Republic of Korea*
[289] *Concordia University Wisconsin, Mequon, WI 53097, USA*

[290] *Department of Electrophysics, National Yang Ming Chiao Tung University, Hsinchu, Taiwan*
[291] *Department of Physics, Rikkyo University, Toshima-ku, Tokyo 171-8501, Japan*

(Dated: August 23, 2022)

Results are presented for a semi-coherent search for continuous gravitational waves from the low-mass X-ray binary Scorpius X-1, using a hidden Markov model (HMM) to allow for spin wandering. This search improves on previous HMM-based searches of Laser Interferometer Gravitational-wave Observatory (LIGO) data by including the orbital period in the search template grid, and by analyzing data from the latest (third) observing run (O3). In the frequency range searched, from 60 to 500 Hz, we find no evidence of gravitational radiation. This is the most sensitive search for Scorpius X-1 using a HMM to date. For the most sensitive sub-band, starting at 256.06Hz, we report an upper limit on gravitational wave strain (at 95% confidence) of $h_0^{95\%} = 6.16 \times 10^{-26}$, assuming the orbital inclination angle takes its electromagnetically restricted value $\iota = 44°$. The upper limits on gravitational wave strain reported here are on average a factor of $\sim 3$ lower than in the O2 HMM search. This is the first Scorpius X-1 HMM search with upper limits that reach below the indirect torque-balance limit for certain sub-bands, assuming $\iota = 44°$.

## I. INTRODUCTION

Rotating neutron stars are promising candidates for continuous-wave searches with terrestrial gravitational wave (GW) detectors such as the second-generation Advanced Laser Interferometer Gravitational-wave Observatory (LIGO) [1–5], Advanced Virgo [4], and the Kamioka Gravitational Wave Detector (KAGRA) [6]. Continuous GWs from neutron stars are emitted by an oscillating quadrupole moment, which can be produced in various ways, including elastic strain [7, 8], magnetic gradients [9–11], $r$-modes [12–14], or nonaxisymmetric circulation of the superfluid interior [15–18]. These mechanisms emit GWs at specific multiples of the spin frequency $f_\star$ [1]. Low-mass X-ray binaries (LMXBs) have been targeted by previous LIGO searches, [19–24] because they may emit GWs relatively strongly while existing in a state of rotational equilibrium, in which the accretion torque balances the GW torque [25–27]. Under torque balance conditions, the characteristic GW strain $h_0$ is proportional to the square root of the X-ray flux, implying that the brightest LMXB, Scorpius X-1 (Sco X-1), is also a strong GW emitter [1, 27].

Continuous-wave searches directed at Sco X-1 have been performed with data from the first (O1) and second (O2) observing runs of LIGO [19–21, 23, 28–31]. No signal has been detected to date, but astrophysically interesting upper limits have been obtained. For O1 a hidden Markov model (HMM) pipeline [29] obtained an upper limit at 95% confidence level of $h_0^{95\%} = 8.3 \times 10^{-25}$ in the 100-200 Hz frequency range, while a cross-correlation (CrossCorr) pipeline [28, 32] achieved $h_0^{95\%} = 2.3 \times 10^{-25}$ in the same frequency range. For O2, the HMM pipeline [21] obtained $h_0^{95\%} = 3.47 \times 10^{-25}$, in the 100-200Hz frequency range, while CrossCorr [23] improved on its O1 results by a factor of $\approx 1.8$. All of these upper limits on $h_0^{95\%}$ are marginalized over the neutron star spin inclination $\iota$, assuming an isotropic prior. If instead one assumes an electromagnetically informed prior, $\iota = 44° \pm 6°$ [33], the O2 upper limits obtained by CrossCorr reduce to $\sim 10^{-26}$ [23]. As with any observation the upper limits are conditional on the signal model. CrossCorr and the HMM assume different phase evolution, so the foregoing $h_0^{95\%}$ values cannot be compared directly (see Section V B), although they are broadly indicative of course. Now, the third observation run (O3), which is longer and more sensitive than O1 and O2, offers an opportunity to repeat the O1 and O2 searches with improved sensitivity. The improved HMM search is the subject of this paper.

Searching for LMXBs presents two challenges. First, $f_\star$ (and hence the GW frequency) wanders stochastically in objects where it is measured electromagnetically, due to fluctuations in the hydromagnetic accretion torque [34–37]. Second, in some LMXBs including Sco X-1, which do not exhibit X-ray pulsations, $f_\star$ is not measured electromagnetically [1, 37]. Hence a GW search must cover a wide band (width $\sim 1$ kHz) looking for an unknown, wandering, quasimonochromatic tone [38, 39]. HMM tracking is a tried and tested method for searches of the above sort, with a long history of practical use in telecommunications [40] and remote sensing [41]. HMM tracking has been used in numerous searches for GWs, e.g. for Sco X-1 in O1 [29] and O2 [21], young supernova remnants in O3 [42], accreting millisecond X-ray pulsars in O2 [22] and O3 [24], all sky searches [43], and long-duration transients [44].

The $\mathcal{J}$-statistic [45], a frequency domain matched filter, is used in tandem with the HMM described in references [21, 29, 45, 46]. The outline of the rest of the paper is as follows. Section II explains briefly the HMM formulation used and the $\mathcal{J}$-statistic. In Section III the search pipeline and parameter space are described. In Sections IV and V, we present the search results and upper limits, respectively. We conclude in Section VI.

* Deceased, August 2020.
† Deceased, April 2021.

## II. HMM ALGORITHM

In Section II A we review the HMM formalism used to track the wandering GW emission frequency from one time step to the next, according to a user-selected set of transition probabilities. For each time-step we calculate the likelihood of a signal being present given the data, via a maximum likelihood matched filter called the $\mathcal{J}$-statistic, which is reviewed in Section II B.

### A. Hidden state structure and automaton

A HMM is a probabilistic finite state automaton characterized by a hidden state variable, $q(t)$, which takes the discrete values $\{q_1, \ldots, q_{N_Q}\}$, and an observable state variable, $o(t)$, which takes the discrete values $\{o_1, \ldots, o_{N_O}\}$. The automaton jumps between states at discrete time epochs $\{t_1, \ldots, t_{N_T}\}$. The probability of being in hidden state $q(t_{n+1})$ at time $t_{n+1}$ depends only upon the state at the previous time step $t_n$. This is known as a Markov process.

To complete the model two matrices are defined. First, the transition probability matrix, $A_{q(t_{n+1})\,q(t_n)}$, which relates the probability of a state $q(t_n)$ to jump to $q(t_{n+1})$, takes the form

$$A_{q(t_{n+1})\,q(t_n)} = \frac{1}{3}\Big[\delta_{[q(t_{n+1})]\,[q(t_n)-\Delta q]} + \delta_{[q(t_{n+1})]\,[q(t_n)]} + \delta_{[q(t_{n+1})]\,[q(t_n)+\Delta q]}\Big], \tag{1}$$

where $\delta_{ij}$ is the Kronecker delta, with $i$ and $j$ given by the terms in square brackets respectively. Eq. (1) defines the signal model as a piece-wise constant function that jumps by $-1, 0$, or 1 frequency bin $\Delta q$ at each discrete transition time. See Section III A for the details on the search frequency bin size. The other matrix is the emission probability matrix $L_{o(t_n)q(t_n)}$ that relates the likelihood of observing $o(t_n)$ if the hidden state variable is $q(t_n)$. $L_{o(t_n)q(t_n)}$ is constructed from the matched-filter $\mathcal{J}$-statistic, which we review in Section II B. In our GW application, $f_\star(t)$ maps onto $q(t)$, noting that $f_\star(t)$ is hidden because it cannot be measured electromagnetically for Sco X-1.

The data, specifically the Fourier transform of the time series output by the detector, map onto $o(t)$. The total observation time $T_{\rm obs}$ is divided into $N_T$ segments of duration $T_{\rm drift}$ rounded down to the nearest integer, i.e. $N_T = \lfloor T_{\rm obs}/T_{\rm drift} \rfloor$. $T_{\rm drift}$ is chosen to prevent $f_\star(t)$ from wandering by more than one frequency bin per time step. The rate of spin wandering is unknown *a priori* in Sco X-1, as $f_\star(t)$ cannot be measured electromagnetically. The observed X-ray flux variability can be used to estimate the stochastic variation in $f_\star(t)$ [38, 47], and from this we make an informed choice of $T_{\rm drift}$, as in previous searches.

The probability that the hidden state follows some path $Q = \{q(t_1), \ldots, q_{t_{N_T}}\}$ given some observed data $O = \{o(t_0), \ldots, o(t_{N_T})\}$ is then given by the product of the transition and emission probabilities for each step, viz

$$P(Q|O) = L_{o(t_{N_T})q(t_{N_T})} A_{q(t_{N_T})q(t_{N_T-1})} \cdots \times L_{o(t_1)q(t_1)} A_{q(t_1)q(t_0)} \Pi_{q(t_0)}, \tag{2}$$

where we define the prior probability of being in some initial state $q(t_0)$ at time $t_0$ as $\Pi_{(t_0)}$. In this paper we assign equal probability to all initial states, with $\Pi_{q(t_0)} = 1/N_Q$.

We seek the path $Q^*$ that maximizes $P(Q|O)$ in Eq. (2). But it is computationally inefficient to consider all the $N_Q^{N_T+1}$ possible paths. A robust and computationally efficient way to find $Q^*$ is the Viterbi algorithm [48]. This recursive algorithm exploits the principle of optimality to find $Q^*$ given $O$. A comprehensive description of the algorithm can be found in Appendix A of Ref. [29].

In this paper we use as detection statistic the log-likelihood of the most likely path $\mathcal{L} = \ln P(Q^*|O)$.

### B. $\mathcal{J}$-statistic

The emission probability $L_{o(t_n)q(t_n)}$ relates the observed data, $o(t_n)$, collected in the interval $t_n \le t \le t_n + T_{\rm drift}$ to the hidden states $q(t_n)$. In this paper, we express $L_{o(t_n)q(t_n)}$ in terms of the $\mathcal{J}$-statistic [21, 45]. The $\mathcal{J}$-statistic is a maximum likelihood, frequency domain, matched-filter which tracks the orbital phase of the neutron star in its binary system. It is an extension of the traditional $\mathcal{F}$-statistic [49], which is a matched filter for a biaxial rotor [50]. The Doppler shift due to the binary motion disperses the $\mathcal{F}$-statistic power into orbital sidebands of the GW carrier frequency. Although the $\mathcal{F}$-statistic can be used to produce matched filters to account for the Doppler shift due to the binary motion, the $\mathcal{J}$-statistic is used for computational efficiency. Section III in Ref. [45] presents the detailed derivation of the $\mathcal{J}$-statistic.

In general, to account for the dispersed power, the $\mathcal{J}$-statistic is constructed from matched filters of the suggestive form

$$G(f) = \mathcal{F}(f) \otimes B(f), \tag{3}$$

with

$$B(f) = \sum_{s=-m}^{m} J_s(2\pi f_0 a_0) \exp(-\imath s \phi_a) \delta\left(f - \frac{s}{P}\right), \tag{4}$$

where $\otimes$ denotes convolution, $J_s(x)$ is the Bessel function of the first kind of order $s$, $m = \mathrm{ceil}\,(2\pi f_0 a_0)$, and $f_0$ is the central frequency of the sub-band (See Section III A for details). Eq. (4) assumes the GW signal is produced by a biaxial rotor in a circular Keplerian orbit, and requires three binary orbital parameters: the projected semi-major axis $a_0$, the orbital phase at a reference time $\phi_a$, and $P$ is the binary orbital period.

## III. SEARCH IMPLEMENTATION

In this section we discuss the practical details of the search. Sections III A and III B define the parameter domain and grid respectively. Section III C sets out the workflow. Section III D justifies the selection of the false alarm probability in terms of the number of search templates. Section III E specifies the primary and secondary data products ingested by the search.

### A. Sco X-1 parameters

The $\mathcal{J}$-statistic depends on the location of the source, described by the right ascension $\alpha$, and declination $\delta$. It also depends on the three binary orbital elements: $P$, $a_0$, and $\phi_a$. The time of passage through the ascending node, $T_{\rm asc}$, is linked to $\phi_a$ via $\phi_a = 2\pi T_{\rm asc}/P \,(\mathrm{mod} 2\pi)$. Henceforth we use $T_{\rm asc}$ instead of $\phi_a$. Some of these parameters have been measured electromagnetically for Sco X-1. Their values and uncertainties are summarized in Table I.

The last electromagnetic measurements [51] for the time of ascension $T_{\rm asc,ref} = 974\,416\,624$ GPS time are dated November 22 04:00:15 GMT 2010, here denoted $T_0$. We forward propagate $T_{\rm asc,ref}$ to the start of O3, $T_{\rm O3,0} = 1238166483$ GPS time, viz.

$$T_{\rm asc,0} = T_{\rm asc,ref} + N_{\rm orb} P_0, \tag{5}$$

where $P_0 = 68\,023.86048$ s is the central value of the orbital period in Table I, and $N_{\rm orb} = \lceil \frac{T_{\rm O3,0} - T_0}{P_0} \rceil$ is the number of full orbits between the reference time $T_0$ and $T_{\rm O3,0}$. The original uncertainties for $T_{\rm asc,ref}$ and $P$ are also propagated using Eq. (5). This is illustrated in Figure 1. The propagation maps the original uncertainty ellipses of $T_{\rm asc,ref}$-$P$ (upper panel in Figure 1) to the present uncertainty ellipses $T_{\rm asc}$-$P$ (lower panel in Figure 1). Propagating the original uncertainties via Eq. (5) creates correlations between the uncertainties of $T_{\rm asc}$ and $P$.

The propagated priors on $T_{\rm asc}$ and $P$ change throughout the search duration as their correlation grows with time. The lower panel of Figure 1 shows the change from the start of O3 marked as solid color lines, to its end, $T_{\rm O3end} = 1269361423$ GPS time, shown as dotted lines. The search has been designed to cover the whole $3\sigma$ region of the propagated $T_{\rm asc}$-$P$ space, from start to end of O3.

For $a_0$, we cover the range $1.45 \leq a_0/(1\,\mathrm{s}) \leq 3.25$, following the electromagnetic measurements presented in [51]. We can write this range equivalently as $\bar{a}_0 \pm 3\sigma_{a_0}$, with $\bar{a}_0 = 2.35$ s and $\sigma_{a_0} = 0.3$ s.

The coherence time is set to $T_{\rm drift} = 10$ d. The latter choice is justified astrophysically: it is the characteristic time-scale of the random walk in $f_\star$ inferred from accretion-driven fluctuations in the X-ray flux of Sco X-1 [19, 38, 47]. It also matches the value used in previous published searches for Sco X-1, enabling direct comparison with historical results [19, 21, 28, 29]. The resolution in frequency space $\Delta f_{\rm drift}$, i.e the size of the frequency bins, is set by the coherence time as $\Delta f_{\rm drift} = 1/(2T_{\rm drift}) = 5.787037 \times 10^{-7}$ Hz.

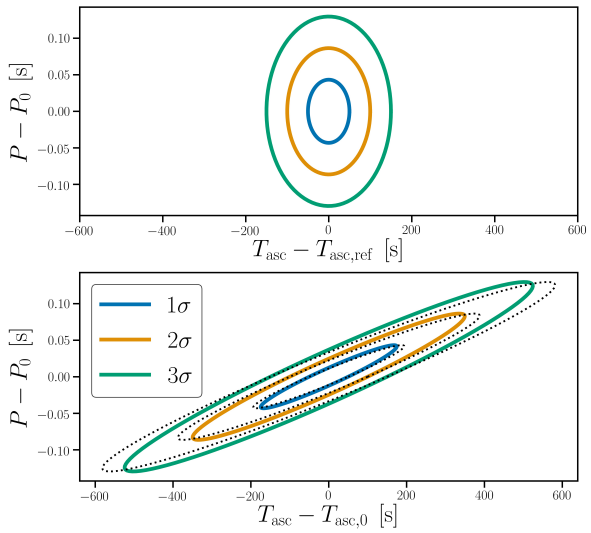


FIG. 1. Uncertainty ellipses corresponding to $1\sigma$ [blue line], $2\sigma$ [yellow line], and $3\sigma$ [green line], for $T_{\rm asc}$ and $P$. The above panel show the curves at the reference time $T_0$, when $T_{\rm asc,ref}$ is uncorrelated with $P_0$ or its uncertainties. The second panel shows the effect of propagating $T_{\rm asc,ref}$ and $P_0$, with their respective uncertainties, to the start of O3 ($T_{\rm O3,0} = 1238166483$ GPS time) [solid lines] or the end of O3 ($T_{\rm O3end} = 1269361423$ GPS time) [black dots]. $T_{\rm asc,0}$ represents the central value of $T_{\rm asc,ref}$ propagated to the start or end of O3; that is, $T_{\rm asc,0}$ is different for the solid and dotted lines. In both panels we have $P_0 = 68\,023.86048$ s.

The range of frequencies to be searched, 60 Hz to 500 Hz, covers the region where LIGO is most sensitive. This frequency range is divided into sub-bands. This eases the manipulation of the data and allows one to approximate $f_0$ in Eq. (4) by the mid-point frequency $\bar{f}$ in each sub-band, accelerating the process of creating each matched filter via Eq. (4) [45]. The sub-bands are designed to contain a number of frequency bins $N_f$ that is a power of two, in order to accelerate the fast Fourier transform involved in calculating the convolution in Eq. (4). For this search we use $N_f = 2^{20}$, setting the sub-band width to $\Delta f_{\rm sub} = N_f \Delta f_{\rm drift} = 0.6068148$ Hz. As such the total number of sub-bands to consider in our search is $N_{\rm sub} = \lceil (500 - 60)\ \mathrm{Hz}/\Delta f_{\rm sub} \rceil = 725$. As the $\mathcal{J}$-statistic is less sensitive farther away from $\bar{f}$, we create sub-bands with an overlap of $\Delta f_{\rm sub}/4$. This way the area with less sensitivity in a sub-band is covered with greater sensitivity in the neighbouring sub-band. All of the parameters discussed in this section are summarized in Table I.

TABLE I. Search parameters and their range. The column headed "EM data" records the availability of electromagnetic measurements in the references in the last column. All parameter ranges include the central value together with $\pm 1\sigma$ uncertainties; values without uncertainties are treated as constants. In the text generally the central values are denoted with the subscript 0, e.g. $P_0$. The time of ascension $T_{\rm asc}$ stands for the value in [51] propagated up to the start of O3, as described in Section III A. As written here $T_{\rm asc}$ and $P$, plus their uncertainties, define a rectangular parameter domain. We only search over the grid points that have support from the propagated priors, defined by all the ellipses in the lower panel of Figure 1; See Section III B for details.

| Parameter | Symbol | Search range | EM data | Reference |
|---|---|---|---|---|
| Right ascension | $\alpha$ | 16 h 19 m 55.0850 s | Y | [52] |
| Declination | $\delta$ | $-15°38'24.9''$ | Y | [52] |
| Orbital inclination angle | $\iota$ | $44 \pm 6°$ | Y | [33] |
| Projected semi-major axis | $a_0$ | $2.35 \pm 0.3$ s | Y | [51] |
| Orbital period | $P$ | $68\,023.86048 \pm 0.0432$ s | Y | [51] |
| GPS time of ascension | $T_{\rm asc}$ | $1\,238\,149\,477.03488 \pm 200$ s | Y | [51] |
| Frequency | $f$ | $60 - 500$ Hz | N | - |

### B. Number and placing of orbital templates

In this subsection we describe the procedure to calculate and place the orbital templates needed to cover the search parameter domain per sub-band.

As explained in Section III A, the forward propagation of the reference $T_{\rm asc,ref}$ increases its uncertainty as a function of $N_{\rm orb}$. To be conservative, we choose to propagate the uncertainties on $T_{\rm asc,ref}$ to the end of O3 with

$$\sigma_{T_{\rm asc}} = \sqrt{\sigma^2_{T_{\rm asc,ref}} + (N_{\rm orb,end}\sigma_P)^2}, \tag{6}$$

where one has $N_{\rm orb,end} = \lceil \frac{T_{\rm O3end} - T_0}{P_0} \rceil$, and $\sigma_{T_{\rm asc,ref}} = 50$ s and $\sigma_P = 0.0432$ s are the uncertainties for $T_{\rm asc,ref}$ and $P$ respectively, the result $\sigma_{T_{\rm asc}} = 200$ s is included in Table I. Although the uncertainties are propagated to the end of O3, the central value for the time of ascension is only propagated to the start of O3, $T_{\rm asc_0} = 1\,238\,149\,477.03488$ s, as shown in Section III A.

We cover the parameter space by using a rectangular grid defined by the limits $(\bar{a}_0 \pm 3\sigma_{a_0}, T_{\rm asc} \pm 3\sigma_{T_{\rm asc_0}}, P_0 \pm 3\sigma_P)$. We set the spacing of the grid points by selecting an acceptable maximum mismatch $\mu_{\rm max}$, following [53]. This mismatch represents the fractional loss in signal-to-noise ratio between the search with the true parameters and the nearest grid point. For the search we use $\mu_{\rm max} = 0.1$. The number of grid points needed to cover the $(a_0, T_{\rm asc}, P)$ space, for a given $\mu_{\rm max}$, are calculated using Eq. (71) of Ref. [53], namely

$$N_{a_0} = \left\lceil 3\sqrt{2}\mu_{\rm max}^{-1/2} f \sigma_{a_0} \right\rceil, \tag{7}$$

$$N_{T_{\rm asc}} = \left\lceil 6\pi^2\sqrt{2}\mu_{\rm max}^{-1/2} f a_0 P^{-1} \sigma_{T_{\rm asc}} \right\rceil, \tag{8}$$

$$N_{\rm P} = \left\lceil \pi^2\sqrt{6}\mu_{\rm max}^{-1/2} f a_0 T_{\rm drift} N_T P^{-2} \sigma_P \right\rceil. \tag{9}$$

| Sub-band (Hz) | $N_{a_0}$ | $N_{T_{\rm asc}}$ | $N_P$ |
|---|---|---|---|
| 60 | 767 | 149 | 5 |
| 160 | 2031 | 394 | 12 |
| 260 | 3296 | 640 | 19 |
| 360 | 4560 | 885 | 27 |
| 460 | 6331 | 1228 | 37 |

TABLE II. Selected sub-bands and corresponding $N_{a_0}, N_{T_{\rm asc}}, N_{\rm P}$ values, using $\mu_{\rm max} = 0.1$. The table serves to illustrate how the number of orbital templates varies across the full frequency band.

For O3 the number of contiguous semi-coherent segments is $N_T = 36$. To be conservative when applying Eqs. (7)-(9), we use the highest frequency in each sub-band for $f$, the highest $a_0 = \bar{a}_0 + 3\sigma_{a_0}$ and the lowest $P = P_0 - 3\sigma_P$. Table II lists the number of grid points in selected sub-bands. For $T_{\rm asc}$ and $P$ we search only the points defined by Eqs. (7)-(9) that lie within the start (color lines) and end (dotted lines) ellipses in the bottom panel of Figure 1.

### C. Workflow

The workflow for the search is illustrated in Figure 2, as a flow chart.

At the outset, the time series from the detector is converted into short Fourier transforms (SFTs) lasting $T_{\rm SFT} = 1800$ s. The corresponding data, for each frequency sub-band, are divided into $N_T$ blocks of duration $T_{\rm drift} = 10$ d. All of the SFTs in a single block are used to calculate an $\mathcal{F}$-statistic *atom* [54] with the fixed parameters $\alpha$ and $\delta$ in Table I. The process is repeated for all the blocks, generating $N_T$ atoms. The $\mathcal{F}$-statistic atoms do not depend on the orbital parameters so they are stored in a look-up table. The steps in this paragraph conclude in the blue parallelogram denoted "$N_T$ $\mathcal{F}$-statistic atoms" in Figure 2.

In every sub-band, each $\mathcal{F}$-statistic atom is fed into the $\mathcal{J}$-statistic in Eq. (4) for a triad of orbital parameters $(a_0, T_{\rm asc}, P)$. The Viterbi algorithm (see [48] or Section II.B of Ref. [45]) finds the optimal frequency path connecting the $\mathcal{J}$-statistic blocks and its associated log likelihood. In Figure 2, the latter steps extend from the orange rectangle "Calculate the $\mathcal{J}$-statistic" up to the blue parallelogram marked "log likelihood and optimal path for $(a_0, T_{\rm asc}, P)_i$".

For a sub-band centered on the frequency $\bar{f}$, the search scans over all binary templates $(a_0, T_{\rm asc}, P)_i$ with $1 \leq i \leq N_{a_0}(\bar{f}) N_{T_{\rm asc}}(\bar{f}) N_P(\bar{f})$, calculated using Eqs. (7)-(9). This step is illustrated as the green oval denoted "Used all templates?" in Figure 2. For each $(a_0, T_{\rm asc}, P)_i$ an optimal path and its associated log likelihood are recorded.

Following the loop over all binary templates, the optimal path with highest log likelihood, denoted $\max(\mathcal{L})$, is selected in the blue parallelogram marked "$\max(\mathcal{L})$ and assoc. optimal path" in Figure 2. If $\max(\mathcal{L})$ is higher than the detection threshold (see Section III D), then the sub-band is recorded as a candidate and passed through a hierarchy of vetoes (see Section IV B), via the "yes" output of the upper green oval.

Sub-bands with $\max(\mathcal{L})$ below the detection threshold are used to calculate GW strain upper limits via the "no" output of the upper green oval. Vetoed sub-bands are not used to calculate GW upper-limits.

### D. False alarm probability and detection threshold

A sub-band is registered as a candidate, when $\max(\mathcal{L})$ exceeds a threshold, $\mathcal{L}_{\rm th}$, corresponding to a user-selected false alarm probability. As the distribution of $\max(\mathcal{L})$ in pure noise is unknown we rely on Monte-Carlo simulations to determine $\mathcal{L}_{\rm th}$ in each sub-band of the search. To estimate the distribution of $\max(\mathcal{L})$ in pure noise, we generate synthetic Gaussian data using the `lalapp_Makefakedata_v5` program in the LIGO Scientific Collaboration Algorithm Library (LALSuite) [55]. The synthetic data are generated for a sub-band centered on the frequency $\bar{f}$, with $\alpha$ and $\delta$ copied from Table I. Then the search workflow described in Section III C is applied. To avoid needless computation, we limit the grid to $N_{a_0} = 322$, $N_{T_{\rm asc}} = 35$, and $N_P = 5$ in every sub-band, independent of $\bar{f}$.

In general $\mathcal{L}_{\rm th}$ depends on the number of generated log likelihoods per sub-band, i.e. $N_{\rm tot} = N_f\, N_{a_0}\, N_{T_{\rm asc}}\, N_P$. We describe the false alarm probability, $\alpha_{N_{\rm tot}}$, of a sub-band with $N_{\rm tot}$ log likelihoods in terms of the probability of a false alarm in a single terminating frequency bin per orbital template, $\alpha$, as

$$\alpha_{N_{\rm tot}} = 1 - (1-\alpha)^{N_{\rm tot}}. \tag{10}$$

The PDF of the log-likelihood per sub-band, $p(\mathcal{L})$, for the most likely path given an orbital template is observed to follow an exponential tail, $p(\mathcal{L}) = A \exp[-\lambda(\mathcal{L} - \mathcal{L}_{\rm tail})]$ in noise. The cut-off $\mathcal{L}_{\rm tail}$, and the $\lambda$-parameter are obtained empirically. From our synthetic Gaussian trials we obtain $\lambda = 0.23$ across all sub-bands. The normalization $A = N_{\rm tail}/N_{\rm tot}$, where $N_{\rm tail}$ is the number of log-likelihoods above $\mathcal{L}_{\rm tail}$, is calculated from the $N_{\rm tot}$ samples used to generate $p(\mathcal{L})$. The probability $\alpha$, in Eq. (10) is given by

$$\alpha = \int_{\mathcal{L}_{\rm th}}^{\infty} p(\mathcal{L}) d\mathcal{L}. \tag{11}$$

Combining $p(\mathcal{L})$, Eq. (10), and Eq. (11) yields for $\mathcal{L}_{\rm th}$

$$\mathcal{L}_{\rm th} = \mathcal{L}_{\rm tail} - \frac{1}{\lambda} \log\left(\frac{\alpha_{N_{\rm tot}}}{N_{\rm tail}}\right), \tag{12}$$

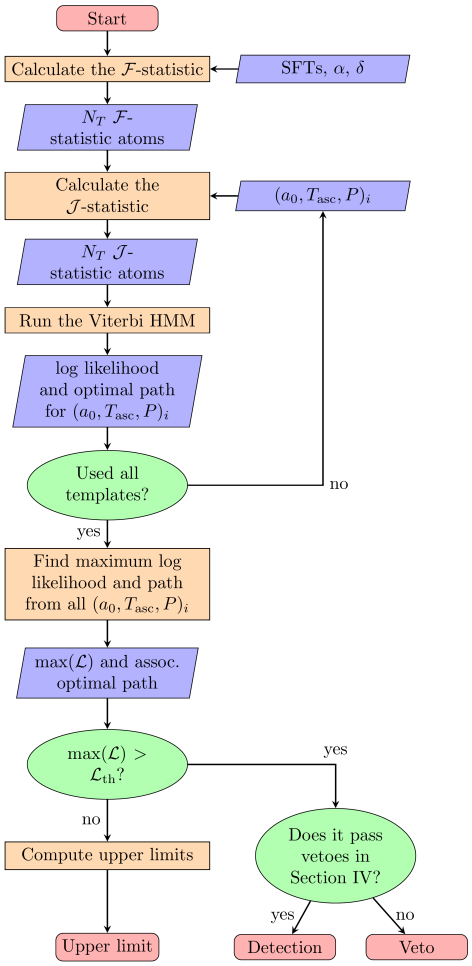


FIG. 2. Flowchart of the search pipeline for a sub-band. The light red octagons are the start and end points, the orange rectangles are processes, the blue parallelograms are input or output data, and the green ovals stand for decision points. The full search repeats the steps in the flowchart for 725 sub-bands from 60Hz to 500Hz.

provided Eq. (10) is Taylor expanded to first order, given $N_{\rm tot} \gg 1$. Note that $\mathcal{L}_{\rm th}$ is an implicit function of the sub-band frequency through $N_{\rm tail}$.

Historically HMM Sco X-1 searches [21, 29] use $\alpha_{N_{\rm tot}} = 0.01$, a choice we adopt here to avoid excessive follow-up of candidates and ease the comparison with previous HMM Sco X-1 searches. A false-alarm probability of 1% per sub-band applied to a total of 725 sub-bands implies we should expect $\sim 7$ false alarms from the search. Searches with electromagnetically constrained $f_\star$ such as Ref. [22] and Ref. [24] allow for $\alpha_{N_{\rm tot}} = 0.3$, given the reduced search space. Appendix A in Ref. [24] presents the detailed procedure to set thresholds using Monte-Carlo simulations.

### E. O3 data

The search uses all the O3 dataset, starting April 1, 2019, 15:00 UTC and finishing March 27, 2020, 17:00 UTC. The dataset is divided in two. The first part (O3a) spans 1 April 2019 to 1 Oct 2019 followed by a month long commissioning break. The second part (O3b) was intended to span 1 November 2019 to 30 April 2020 but was suspended in March 2020 due to the COVID-19 coronavirus pandemic. SFTs are generated from the "C01 calibrated self-gated" dataset, specifically designed to remove loud glitches from the strain data, following the procedure in Ref. [56].

Due to the month-long commissioning break between O3a and O3b, two out of $N_T$ segments have no SFTs. The two segments are dated October 8, 2019, 15:00 UTC and October 15, 2019, 15:00 UTC, respectively. We replace them by segments with uniform log-likelihood across all frequency bins, to allow the HMM to connect data from O3a with data from O3b while accommodating spin wandering. Every time atoms are created, such as in Sections III D, IV B 2 and IV B, the relevant missing atoms are replaced with uniform log-likelihood atoms.

## IV. O3 ANALYSIS

### A. Candidates

The results of the search are plotted in Figure 3. On the horizontal axis we show the terminating frequency bin of the optimal path, i.e $q^*(t_{N_T})$ per sub-band, that satisfies $\max(\mathcal{L}) > \mathcal{L}_{\rm th}$, defining preliminary signal candidates. On the vertical axes we graph the orbital parameters $a_0$ (left panel), $T_{\rm asc}$ (middle panel), and $P$ (right panel).

Figure 3 contains 35 candidates with $\max(\mathcal{L}) > \mathcal{L}_{\rm th}$. To eliminate false alarms we use the hierarchy of vetoes employed in Ref. [21]. The vetoes discard candidates that (i) lie near an instrumental noise line (known line veto) or (ii) appear in one interferometer (IFO) but not the other (single IFO veto). In previous searches other vetoes, e.g. candidates that appear in half of the observation time ($T_{\rm obs}/2$ veto), have been used in addition to (i) and (ii) [21, 22, 24, 29, 42]. Additional vetoes are unnecessary in this paper; all but one of the candidates are vetoed by (i) and (ii), and the survivor is eliminated by other means, as discussed below. The outcomes of the vetoes in the 35 sub-bands containing outliers are recorded in Table III.

The sole candidate that passes vetoes (i) and (ii), contained in the sub-band starting at 60.05 Hz, is suspiciously close to the known 60 Hz noise line due to the United States of America power grid [57]. Additionally, several other candidates appear near harmonics of 60.05 Hz, for instance 119.52 Hz and 179.60 Hz. When we search the sub-band using the C01 calibrated self-gated 60 Hz subtracted dataset, which uses the algorithm described in Ref. [58] to subtract the 60 Hz noise line, the candidate disappears.

### B. Vetoes

#### 1. *Known lines*

Narrowband noise features in the IFO are caused by a plethora of reasons, such as the suspension system or the electricity grid [59, 60]. As noise lines artificially increase the output of the $\mathcal{F}$-statistic, sub-bands that contain them tend to be flagged as candidates. In response, we veto any candidate whose optimal frequency path $f(t_i)$ satisfies

$$|f(t_i) - f_{\rm line}| < \frac{2\pi a_0 f_{\rm line}}{P}, \tag{13}$$

for any epoch $t_i$ in the search. Here $f_{\rm line}$ is the frequency of the noise line. We refer to the vetted known lines list in Ref. [61]. This test vetoes 30 out of the 35 candidates. We note that the number of remaining candidates, after eliminating those caused by noise lines, is consistent with our original number of expected candidates.

#### 2. *Single IFO*

A plausible astrophysical signal that has escaped detection in prior searches would likely be weak enough to need data from both IFOs to be detectable, or strong enough to be seen in both, given their comparable sensitivities in most frequency bands. In contrast, instrumental artifacts are unlikely to appear simultaneously in both IFOs. Let $\max(\mathcal{L})_{\rm a}$ and $\max(\mathcal{L})_{\rm b} > \max(\mathcal{L})_{\rm a}$ denote the log likelihoods in each IFO, and let $\max(\mathcal{L})_\cup$ denote the log likelihood of the original candidate. There are four possible outcomes:

1. If one finds $\max(\mathcal{L})_{\rm a} < \mathcal{L}_{\rm th}$ and $\max(\mathcal{L})_{\rm b} > \max(\mathcal{L})_\cup$, and the optimal path, $f_b(t_i)$, associated with $\max(\mathcal{L})_{\rm b}$, satisfies

$$|f_\cup(t_i) - f_b(t_i)| < \frac{2\pi a_0 f_\cup}{P} \tag{14}$$

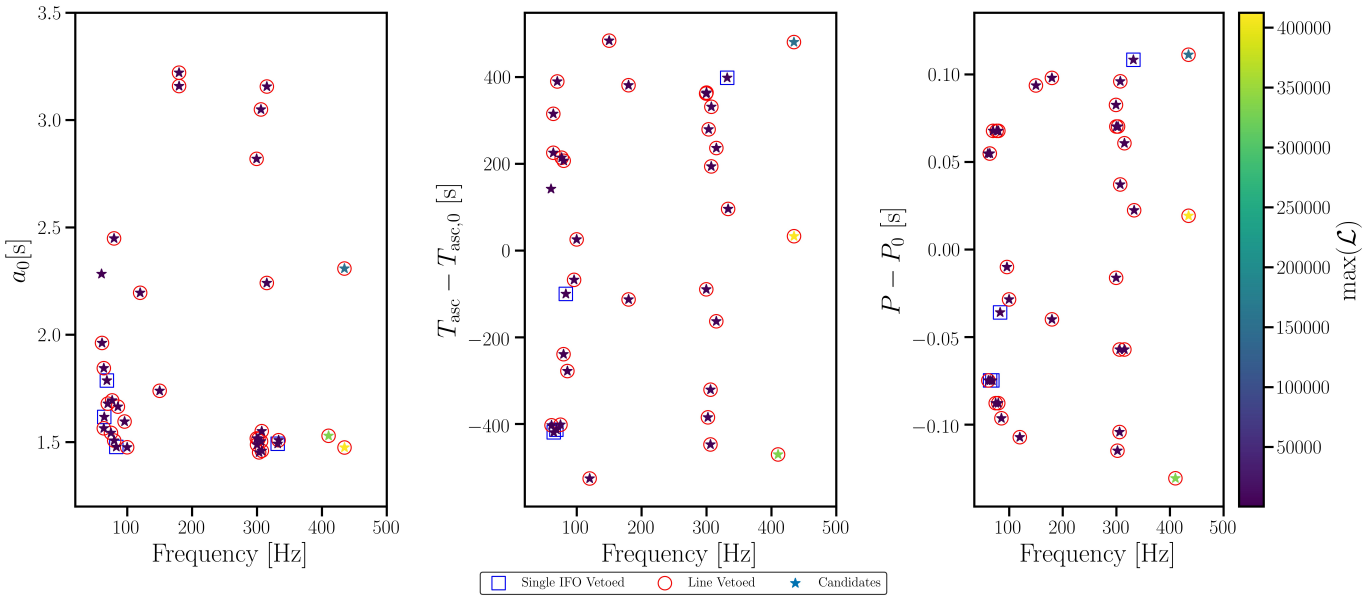


FIG. 3. Candidates plotted as a function of their terminating frequency bin $q^*(t_{N_T})$ (horizontal axis, units in Hz) and the orbital parameters $a_0$ (vertical axis in left panel, units in s), offset from the central time of ascension $T_{\rm asc} - T_{\rm asc_0}$ (vertical axis in central panel; units in s) and offset from the central period $P - P_0$ (vertical axis in right panel; units in s). The color scale indicates the max($\mathcal{L}$) obtained for the candidate. Candidates marked with purple squares are eliminated by the single IFO veto, while red circles mark the ones eliminated by the known lines veto. The candidate with no marking survives both the single IFO and known lines vetoes, but is eliminated by its absence when using noise-subtracted data (See Section IV A).

for any epoch $t_i$ in the search, where $f_\cup(t_i)$ is the optimal path associated with $\max(\mathcal{L})_\cup$ then the candidate is consistent with an instrumental artifact in detector $b$. It is vetoed.

2. If one finds $\max(\mathcal{L})_{\rm a} < \mathcal{L}_{\rm th}$ and $\max(\mathcal{L})_{\rm b} > \max(\mathcal{L})_\cup$ but the candidate does not satisfy Eq. (14), then it is saved for further post-processing. Such a candidate could be a faint astrophysical signal which needs both IFOs to be detected.

3. If one finds $\max(\mathcal{L})_{\rm a} > \mathcal{L}_{\rm th}$ and $\max(\mathcal{L})_{\rm b} > \mathcal{L}_{\rm th}$, then the candidate could be a strong astrophysical signal. It could also imply a common noise source in both detectors. The candidate is flagged for post-processing.

4. If one finds $\max(\mathcal{L})_{\rm a} < \mathcal{L}_{\rm th}$ and $\max(\mathcal{L})_{\rm b} < \max(\mathcal{L})_\cup$, the candidate could be a weak astrophysical signal that needs both detectors to appear above threshold. This candidate is also saved for post-processing.

This test vetoes four out of the remaining five candidates, with the last candidate eliminated by its non-appearance in noise-subtracted data, as discussed in Section IV A.

## V. FREQUENTIST UPPER LIMITS

### A. Procedure

Sub-bands without candidates are used to place upper limits on the gravitational wave strain detectable at a 95% confidence level, $h_0^{95\%}$. We use the approach in the historical HMM Sco X-1 searches [21, 29] to set frequentist upper limits. This is done to facilitate comparison with previous upper limits.

To capture the variation of the wave strain as a function of the inclination angle $\iota$, we define the effective strain [47]

$$h_0^{\rm eff} = h_0 2^{-1/2}\{\left[(1+\cos^2\iota)/2\right]^2 + \cos^2\iota\}^{1/2}. \qquad (15)$$

We note that Eq. (15) allows us to re-scale $h_0^{95\%}$ for the circularly polarized case, $|\cos\iota| = 1$, to any other inclination angle $\iota$. For example if we assume the electromagnetically measured inclination of Sco X-1 orbit as $\iota = 44°$ then Eq. (15) yields $h_0^{\rm eff,95\%} = 1.35 h_0^{95\%}$.

To set frequentist upper limits in a sub-band with central frequency $\bar{f}$, we start by generating 100 copies of the O3 data for this sub-band. A Sco X-1-like signal, i.e using the astrophysical parameters in Table I, is injected into each copy of the sub-band. The parameters $\{\psi, a_0, T_{\rm asc}, P\}_{\rm inj}$ used to create the injected signal are drawn from uniform distributions within the range given by their respective $3\sigma$ error bars. We make sure the in-

TABLE III. Candidates for the O3 search. The first column corresponds to the minimum frequency in the sub-band that contains the candidate. The second column is the log likelihood of the candidate. The other columns record the outcome of the two vetoes used in Section IV B 1 and IV B 2. A candidate that passes or fails a veto is marked with a ✓or **X** respectively. H and L are the Hanford-only and Livingston-only $\max(\mathcal{L})$ values. The remaining candidate, contained in the 60.05 Hz sub-band, is eliminated when using the "C01 calibrated self-gated 60 Hz subtracted" dataset.

| Sub-band (Hz) | $\max(\mathcal{L})/10^3$ | Known lines veto | Single IFO veto |
|---|---|---|---|
| 60.05 | 0.45 | ✓ | ✓; H:398.58, L:427.97 |
| 60.66 | 0.40 | **X** | - |
| 63.09 | 1.73 | **X** | - |
| 63.70 | 1.39 | **X** | - |
| 64.30 | 0.39 | ✓ | **X** |
| 67.94 | 0.37 | ✓ | **X** |
| 69.76 | 0.60 | **X** | - |
| 74.62 | 4.33 | **X** | - |
| 76.44 | 0.35 | **X** | - |
| 78.87 | 0.35 | **X** | - |
| 79.47 | 0.46 | **X** | - |
| 82.51 | 0.53 | ✓ | **X** |
| 84.93 | 0.41 | **X** | - |
| 95.25 | 0.56 | **X** | - |
| 99.50 | 1.35 | **X** | - |
| 119.52 | 0.64 | **X** | - |
| 149.26 | 0.47 | **X** | - |
| 178.99 | 0.43 | **X** | - |
| 179.60 | 0.59 | **X** | - |
| 298.53 | 1.18 | **X** | - |
| 299.14 | 2.81 | **X** | - |
| 299.75 | 0.38 | **X** | - |
| 301.57 | 3.75 | **X** | - |
| 302.78 | 4.26 | **X** | - |
| 305.21 | 2.34 | **X** | - |
| 305.81 | 4.79 | **X** | - |
| 306.42 | 0.59 | **X** | - |
| 307.03 | 5.21 | **X** | - |
| 314.31 | 3.00 | **X** | - |
| 314.92 | 1.50 | **X** | - |
| 331.30 | 6.40 | ✓ | **X** |
| 332.51 | 0.45 | **X** | - |
| 409.58 | 332.67 | **X** | - |
| 433.85 | 155.83 | **X** | - |
| 434.46 | 412.41 | **X** | - |
| Total: 35 | | | |

jected $T_{\rm asc,inj}$ and $P_{\rm inj}$ values lie inside the propagated priors shown in Figure 1, second panel. The injected frequency $f_{\rm inj}$ is uniformly selected from the interval $\bar{f} \pm \delta f$ with $\delta f = 0.05$ Hz. The interval $\bar{f} \pm \delta f$ is chosen for simplicity. The initial value of $h_0$ is chosen such that there is at least one frequency path with $\max(\mathcal{L}) > \mathcal{L}_{\rm th}$. We progressively reduce $h_0$, holding $\{\psi, a_0, T_{\rm asc}, P\}_{\rm inj}$ constant, until the signal is no longer detectable. We record the last detectable amplitude as $h_{0\,\min i}$. The procedure is repeated for all copies of the sub-band, choosing a new set of injection parameters $\{\psi, a_0, T_{\rm asc}, P\}_{\rm inj}$ per copy. Finally $\{h_{0\,\min 1}, ..., h_{0\,\min 100}\}$ are sorted in ascending order and the 95th becomes $h_0^{95\%}$. The injections have $|\cos\iota| = 1$, so we use Eq. (15) to convert $h_0^{95\%}$ to other polarizations.

### B. Upper limits

The limits on $h_0^{95\%}$ are plotted in Figure 4. We present three cases, as in Ref. [21]: circular polarization $\iota = 0$ (blue dots in Figure 4), $\iota = 44°$ (following the electromagnetic measurements in Ref. [51]; denoted by green dots in Figure 4), and unknown polarization (orange dots in Figure 4). In the latter context, unknown polarization means we marginalize over all possible polarizations assuming a uniform distribution in $\cos\iota$ from $-1$ to 1.

The upper limits from the O3 search are on average $\sim 3$ times lower than those from the O2 HMM search [21]. For the sub-band starting at 256.06 Hz we obtain the lowest $h_0^{95\%}$, given by $4.56 \times 10^{-26}$, $6.16 \times 10^{-26}$, and $9.41 \times 10^{-26}$ for circular, electromagnetically restricted ($\iota = 44°$) and unknown polarizations, respectively. Com-

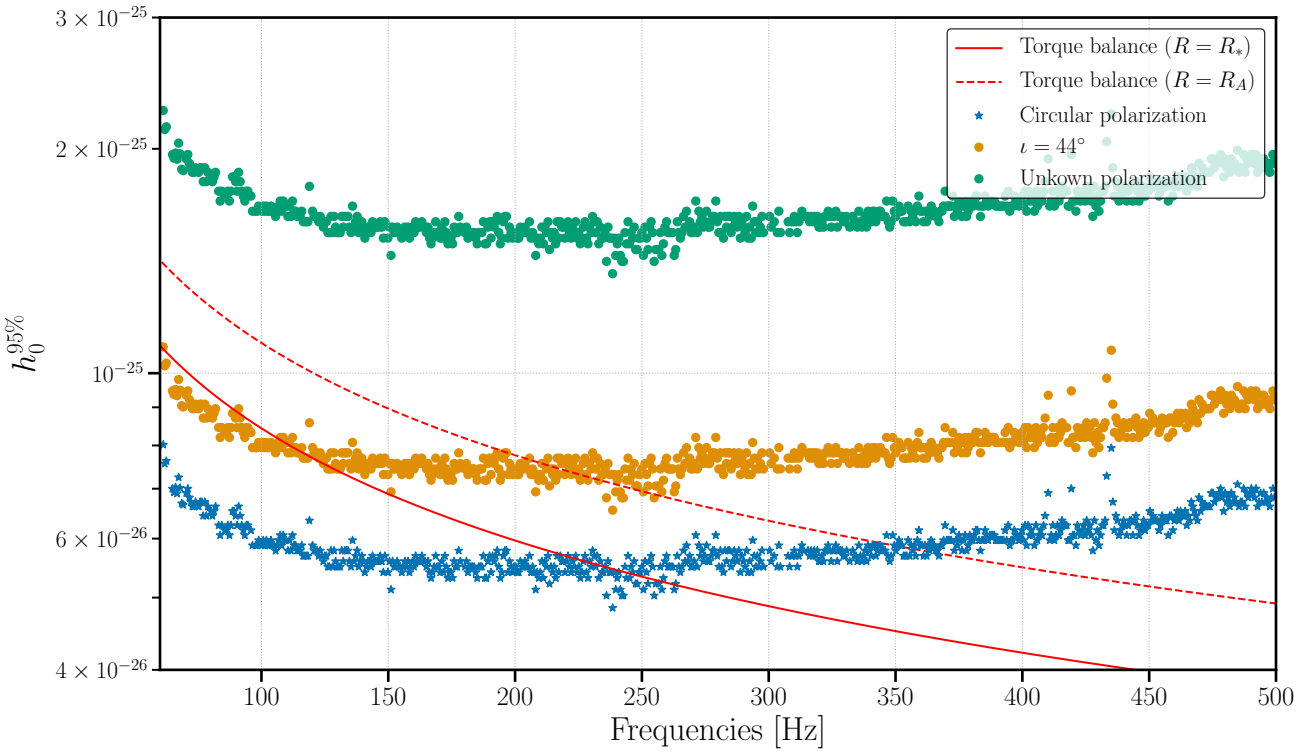


FIG. 4. Frequentist effective wave strain upper limits at 95% confidence as a function of sub-band frequency, for three scenarios: circular polarization with $\iota = 0$ (blue stars), $\iota \approx 44°$ based on the electromagnetic measurements (see Ref. [51]; orange dots), and a flat prior on $\cos\iota$ (green dots). Indirect torque-balance upper limits (see Section V C) for two torque lever arms are also shown: the stellar radius (red solid line) and the Alfvén radius (dashed red line).

pared to the most sensitive sub-bands in previous HMM Sco X-1 searches the lowest $h_0^{95\%}$ is a factor of $\sim 13$ lower than in O1 data [29] and $\sim 3$ lower than in O2 data [21].

It is tempting to compare the results presented in this section with the results of searches with other pipelines, such as CrossCorr O1 [28] and O2 [23]. Such comparisons can be broadly indicative, if done informally. However, the $h_0^{95\%}$ values output by different pipelines cannot be compared directly, when the pipelines assume different phase models, as foreshadowed in Section I. The phase evolution assumed by CrossCorr is given by Eq. (4.15) in Ref. [20], viz. $\Phi_K = \Phi_0 + 2\pi f_0\{t_K - d_K - a_0 \sin[2\pi(t_K - t_{\rm asc})/P]\}$, where $K$ indexes jointly the detector and the selected time interval, with $t_K$ the midpoint of the latter, and $d_K$ is the projected distance from the solar system barycenter to the detector. In previously published CrossCorr implementations [20, 23, 28, 32], it is assumed that $f_0$ stays constant throughout the total observation time $T_{\rm obs}$. Section V A of Ref. [20] explores how the foregoing phase evolution can be generalized in future CrossCorr implementations. On the other hand, the HMM executes an unbiased random walk in $f(t)$, which is piecewise-constant in the coherent blocks $t_n \le t \le t_n + T_{\rm drift}$, as presented in Section II A. The different phase evolution for CrossCorr and the HMM translates into upper limits that are specific to the two different sets of phase paths.

### C. Torque-balance upper limit

Torque-balance assumes the spin-down torque due to gravitational wave emission balances the accretion spin-up torque. From this assumption theoretical upper limits on gravitational wave strain can be estimated from X-ray observations. Following Eq. (4) in Ref. [23], the amplitude of the GW signal produced in torque equilibrium, $h_0^{\rm eq}$, is

$$h_0^{\rm eq} = 3.4 \times 10^{-26} \left(\frac{R}{10{\rm km}}\right)^{1/2} \left(\frac{1.4M_\odot}{M}\right)^{1/4} \left(\frac{r_m}{10{\rm km}}\right)^{1/4} \times \left(\frac{F_X}{3.9 \times 10^{-7}{\rm erg\,cm^{-2}s^{-1}}}\right)^{1/2} \left(\frac{600{\rm Hz}}{f_{\rm GW}}\right)^{1/2}. \quad (16)$$

In Eq. (16), $F_X$ is the X-ray flux, $M$ is the fiducial neutron star mass, $r_m$ is the lever arm, $R$ is the neutron

star radius and $f_{\rm GW}$ is the GW frequency. Eq. (16) assumes the maximum accretion luminosity is completely radiated as X-rays, i.e. $X = 1$ in Eq. (4) of Ref. [23]. To calculate Eq. (16), we use $r_m = R = 10$ km, plotted as a solid red line in Figure 4, or $r_m = R_A$, where $R_A$ is the Alfvén radius, which corresponds approximately to the inner edge of the accretion disk [29, 36]. This is given by

$$R_A = 35 \left(\frac{B_\star}{10^9 G}\right)^{1/4} \left(\frac{R}{10\text{km}}\right)^{12/7} \times \left(\frac{1.4 M_\odot}{M}\right)^{1/7} \left(\frac{10^{-8} M_\odot \text{yr}^{-1}}{\dot{M}}\right)^{2/7} \text{km}, \quad (17)$$

where $B_\star$ is the polar magnetic field strength at the stellar surface, $G$ is Newton's gravitational constant, and $\dot{M}$ is the accretion rate set to the Eddington limit $2 \times 10^{-8} M_\odot \text{yr}^{-1}$, for a fiducial neutron star with mass $M = 1.4 M_\odot$ and radius $R = 10$ km [63, 64]. This limit is plotted in Figure 4 as the dashed red line.

The electromagnetic inclination $\iota = 44°$ produces upper limits that dip under the theoretical torque-balance limits (red lines in Figure 4) for the first time in the HMM Sco X-1 search history. The CrossCorr search pipeline achieved this milestone in the O2 search; see Figure 1 in Ref. [23]. Again, the reader is reminded that different pipelines assume different signal models, and upper limits conditional on different signal models cannot be compared directly.

## VI. CONCLUSIONS

In this paper we search the LIGO O3 data for continuous GWs from the LMXB Sco X-1, using a hidden Markov model, combined with the maximum-likelihood $\mathcal{J}$-statistic and a binary template grid that includes the projected semi major axis $a_0$, time of ascension $T_{\rm asc}$ and orbital period $P$. The binary orbital elements are constrained via electromagnetic observations, but the spin frequency is unknown. Monte-Carlo simulations are used to establish a detection threshold, $\mathcal{L}_{\rm th}$, with a false alarm probability $\alpha_{N_{\rm tot}} = 0.01$, per sub-band. The search is conducted in the range 60 Hz to 500 Hz, partitioned into sub-bands of width $\Delta f_{\rm sub} = 0.606$ Hz. The sub-bands with an optimal path satisfying $\max(\mathcal{L}) > \mathcal{L}_{\rm th}$ are passed through a hierarchy of vetoes. One candidate survives the vetoes, but this candidate is eliminated when using the "C01 calibrated self-gated 60 Hz subtracted" dataset.

The most sensitive sub-band, starting at 256.06 Hz, yields $h_0^{95\%} = 4.56 \times 10^{-26}, 6.16 \times 10^{-26}$, and $9.41 \times 10^{-26}$ for circular, electromagnetically restricted ($\iota = 44°$) and unknown polarizations, respectively.

The above results improve on the two previous HMM Sco X-1 searches [21, 29] by using data from O3 and including the orbital period $P$ in the searched template grid. For comparison, the most sensitive sub-band in the O2 HMM search, 194.6 Hz, obtained $h_0^{95\%} = 1.42 \times 10^{-25}$ for $\iota = 0$ [21], while for the same sub-band and polarization the present search obtains $h_0^{95\%} = 5.40 \times 10^{-26}$. On average our upper limits are a factor of $\sim 3$ below the O2 HMM results. The present search sets the lowest upper-limits for the HMM searches, beating for first time the torque-balance limit for the electromagnetically restricted $\iota = 44°$ case.

Other LMXBs are not as bright in X-rays as Sco X-1, but they are important targets too. Some LMXBs emit X-ray pulsations, so that $f_\star$ is measured to high precision electromagnetically, an important advantage. However the gravitational wave frequency emitted by such objects may be displaced from $f_\star$ and wander randomly with respect to it. An HMM-based search is well placed to track such wandering. Searches for LMXBs with electromagnetically-constrained rotation frequencies have been performed in O2 [22] and O3 [24] data. Ref. [24] reported strain upper limits in the range $5.1 \times 10^{-26} \leq h_0^{95\%} \leq 1.1 \times 10^{-25}$ for its 20 candidates. Such searches offer considerable promise in future observing runs.

## VII. ACKNOWLEDGMENTS

This material is based upon work supported by NSF's LIGO Laboratory which is a major facility fully funded by the National Science Foundation. The authors also gratefully acknowledge the support of the Science and Technology Facilities Council (STFC) of the United Kingdom, the Max-Planck-Society (MPS), and the State of Niedersachsen/Germany for support of the construction of Advanced LIGO and construction and operation of the GEO 600 detector. Additional support for Advanced LIGO was provided by the Australian Research Council. The authors gratefully acknowledge the Italian Istituto Nazionale di Fisica Nucleare (INFN), the French Centre National de la Recherche Scientifique (CNRS) and the Netherlands Organization for Scientific Research (NWO), for the construction and operation of the Virgo detector and the creation and support of the EGO consortium. The authors also gratefully acknowledge research support from these agencies as well as by the Council of Scientific and Industrial Research of India, the Department of Science and Technology, India, the Science & Engineering Research Board (SERB), India, the Ministry of Human Resource Development, India, the Spanish Agencia Estatal de Investigación (AEI), the Spanish Ministerio de Ciencia e Innovación and Ministerio de Universidades, the Conselleria de Fons Europeus, Universitat i Cultura and the Direcció General de Política Universitaria i Recerca del Govern de les Illes Balears, the Conselleria d'Innovació, Universitats, Ciència i Societat Digital de la Generalitat Valenciana and the CERCA Programme Generalitat de Catalunya, Spain, the National Science Centre of Poland and the European Union – European Regional Development Fund; Foundation for Polish Science (FNP), the Swiss National Science Foun-

dation (SNSF), the Russian Foundation for Basic Research, the Russian Science Foundation, the European Commission, the European Social Funds (ESF), the European Regional Development Funds (ERDF), the Royal Society, the Scottish Funding Council, the Scottish Universities Physics Alliance, the Hungarian Scientific Research Fund (OTKA), the French Lyon Institute of Origins (LIO), the Belgian Fonds de la Recherche Scientifique (FRS-FNRS), Actions de Recherche Concertées (ARC) and Fonds Wetenschappelijk Onderzoek – Vlaanderen (FWO), Belgium, the Paris Île-de-France Region, the National Research, Development and Innovation Office Hungary (NKFIH), the National Research Foundation of Korea, the Natural Science and Engineering Research Council Canada, Canadian Foundation for Innovation (CFI), the Brazilian Ministry of Science, Technology, and Innovations, the International Center for Theoretical Physics South American Institute for Fundamental Research (ICTP-SAIFR), the Research Grants Council of Hong Kong, the National Natural Science Foundation of China (NSFC), the Leverhulme Trust, the Research Corporation, the Ministry of Science and Technology (MOST), Taiwan, the United States Department of Energy, and the Kavli Foundation. The authors gratefully acknowledge the support of the NSF, STFC, INFN and CNRS for provision of computational resources. This work was supported by MEXT, JSPS Leading-edge Research Infrastructure Program, JSPS Grant-in-Aid for Specially Promoted Research 26000005, JSPS Grant-in-Aid for Scientific Research on Innovative Areas 2905: JP17H06358, JP17H06361 and JP17H06364, JSPS Core-to-Core Program A. Advanced Research Networks, JSPS Grant-in-Aid for Scientific Research (S) 17H06133 and 20H05639 , JSPS Grant-in-Aid for Transformative Research Areas (A) 20A203: JP20H05854, the joint research program of the Institute for Cosmic Ray Research, University of Tokyo, National Research Foundation (NRF), Computing Infrastructure Project of KISTI-GSDC, Korea Astronomy and Space Science Institute (KASI), and Ministry of Science and ICT (MSIT) in Korea, Academia Sinica (AS), AS Grid Center (ASGC) and the Ministry of Science and Technology (MoST) in Taiwan under grants including AS-CDA-105-M06, Advanced Technology Center (ATC) of NAOJ, and Mechanical Engineering Center of KEK

[1] K. Riles, Gravitational waves: Sources, detectors and searches, Progress in Particle and Nuclear Physics **68**, 1 (2013), arXiv:1209.0667 [hep-ex].
[2] G. M. Harry and LIGO Scientific Collaboration, Advanced LIGO: the next generation of gravitational wave detectors, Classical and Quantum Gravity **27**, 084006 (2010).
[3] F. Acernese, M. Agathos, K. Agatsuma, D. Aisa, N. Allemandou, A. Allocca, J. Amarni, P. Astone, G. Balestri, G. Ballardin, and et al., Advanced Virgo: a second-generation interferometric gravitational wave detector, Classical and Quantum Gravity **32**, 024001 (2015), arXiv:1408.3978 [gr-qc].
[4] LIGO Scientific Collaboration, J. Aasi, B. P. Abbott, R. Abbott, T. Abbott, M. R. Abernathy, K. Ackley, C. Adams, T. Adams, P. Addesso, and et al., Advanced LIGO, Classical and Quantum Gravity **32**, 074001 (2015), arXiv:1411.4547 [gr-qc].
[5] N. Andersson, V. Ferrari, D. I. Jones, K. D. Kokkotas, B. Krishnan, J. S. Read, L. Rezzolla, and B. Zink, Gravitational waves from neutron stars: promises and challenges, General Relativity and Gravitation **43**, 409 (2011), arXiv:0912.0384 [astro-ph.SR].
[6] Kagra Collaboration, T. Akutsu, M. Ando, K. Arai, Y. Arai, S. Araki, A. Araya, N. Aritomi, H. Asada, Y. Aso, and et al., KAGRA: 2.5 generation interferometric gravitational wave detector, Nature Astronomy **3**, 35 (2019), arXiv:1811.08079 [gr-qc].
[7] G. Ushomirsky, C. Cutler, and L. Bildsten, Deformations of accreting neutron star crusts and gravitational wave emission, MNRAS **319**, 902 (2000), arXiv:astro-ph/0001136 [astro-ph].
[8] N. K. Johnson-McDaniel and B. J. Owen, Maximum elastic deformations of relativistic stars, Phys. Rev. D **88**, 044004 (2013), arXiv:1208.5227 [astro-ph.SR].
[9] C. Cutler, Gravitational waves from neutron stars with large toroidal B fields, Phys. Rev. D **66**, 084025 (2002), arXiv:gr-qc/0206051 [gr-qc].
[10] A. Mastrano, A. Melatos, A. Reisenegger, and T. Akgün, Gravitational wave emission from a magnetically deformed non-barotropic neutron star, MNRAS **417**, 2288 (2011), arXiv:1108.0219 [astro-ph.HE].
[11] P. D. Lasky and A. Melatos, Tilted torus magnetic fields in neutron stars and their gravitational wave signatures, Phys. Rev. D **88**, 103005 (2013), arXiv:1310.7633 [astro-ph.HE].
[12] J. S. Heyl, Low-Mass X-Ray Binaries May Be Important Laser Interferometer Gravitational-Wave Observatory Sources After All, ApJ **574**, L57 (2002).
[13] P. Arras, E. E. Flanagan, S. M. Morsink, A. K. Schenk, S. A. Teukolsky, and I. Wasserman, Saturation of the r-Mode Instability, ApJ **591**, 1129 (2003), arXiv:astro-ph/0202345 [astro-ph].
[14] R. Bondarescu, S. A. Teukolsky, and I. Wasserman, Spinning down newborn neutron stars: Nonlinear development of the r-mode instability, Phys. Rev. D **79**, 104003 (2009), arXiv:0809.3448 [astro-ph].
[15] C. Peralta, A. Melatos, M. Giacobello, and A. Ooi, Gravitational Radiation from Nonaxisymmetric Spherical Couette Flow in a Neutron Star, ApJ **644**, L53 (2006), arXiv:gr-qc/0604123 [gr-qc].
[16] C. A. van Eysden and A. Melatos, Gravitational radiation from pulsar glitches, Classical and Quantum Gravity **25**, 225020 (2008), arXiv:0809.4352 [gr-qc].
[17] M. F. Bennett, C. A. van Eysden, and A. Melatos, Continuous-wave gravitational radiation from pulsar glitch recovery, MNRAS **409**, 1705 (2010), arXiv:1008.0236 [astro-ph.SR].

[18] A. Melatos, J. A. Douglass, and T. P. Simula, Persistent Gravitational Radiation from Glitching Pulsars, ApJ **807**, 132 (2015).

[19] J. Aasi, B. P. Abbott, R. Abbott, T. Abbott, M. R. Abernathy, F. Acernese, K. Ackley, C. Adams, T. Adams, P. Addesso, and et al., Directed search for gravitational waves from Scorpius X-1 with initial LIGO data, Phys. Rev. D **91**, 062008 (2015), arXiv:1412.0605 [gr-qc].

[20] J. T. Whelan, S. Sundaresan, Y. Zhang, and P. Peiris, Model-based cross-correlation search for gravitational waves from Scorpius X-1, Phys. Rev. D **91**, 102005 (2015), arXiv:1504.05890 [gr-qc].

[21] B. P. Abbott, R. Abbott, T. D. Abbott, S. Abraham, F. Acernese, K. Ackley, C. Adams, R. X. Adhikari, V. B. Adya, C. Affeldt, and et al., Search for gravitational waves from Scorpius X-1 in the second Advanced LIGO observing run with an improved hidden Markov model, Phys. Rev. D **100**, 122002 (2019), arXiv:1906.12040 [gr-qc].

[22] H. Middleton, P. Clearwater, A. Melatos, and L. Dunn, Search for gravitational waves from five low mass x-ray binaries in the second Advanced LIGO observing run with an improved hidden Markov model, Phys. Rev. D **102**, 023006 (2020), arXiv:2006.06907 [astro-ph.HE].

[23] Y. Zhang, M. A. Papa, B. Krishnan, and A. L. Watts, Search for Continuous Gravitational Waves from Scorpius X-1 in LIGO O2 Data, ApJ **906**, L14 (2021), arXiv:2011.04414 [astro-ph.HE].

[24] The LIGO Scientific Collaboration, the Virgo Collaboration, the KAGRA Collaboration, R. Abbott, T. D. Abbott, F. Acernese, K. Ackley, C. Adams, N. Adhikari, R. X. Adhikari, and et al., Search for continuous gravitational waves from 20 accreting millisecond X-ray pulsars in O3 LIGO data, arXiv e-prints , arXiv:2109.09255 (2021), arXiv:2109.09255 [astro-ph.HE].

[25] J. Papaloizou and J. E. Pringle, Gravitational radiation and the stability of rotating stars., MNRAS **184**, 501 (1978).

[26] R. V. Wagoner, Gravitational radiation from accreting neutron stars, ApJ **278**, 345 (1984).

[27] L. Bildsten, Gravitational Radiation and Rotation of Accreting Neutron Stars, ApJ **501**, L89 (1998), arXiv:astro-ph/9804325 [astro-ph].

[28] B. P. Abbott, R. Abbott, T. D. Abbott, F. Acernese, K. Ackley, C. Adams, T. Adams, P. Addesso, R. X. Adhikari, V. B. Adya, and et al., Upper Limits on Gravitational Waves from Scorpius X-1 from a Model-based Cross-correlation Search in Advanced LIGO Data, ApJ **847**, 47 (2017), arXiv:1706.03119 [astro-ph.HE].

[29] B. P. Abbott, R. Abbott, T. D. Abbott, F. Acernese, K. Ackley, C. Adams, T. Adams, P. Addesso, R. X. Adhikari, V. B. Adya, and et al., Search for gravitational waves from Scorpius X-1 in the first Advanced LIGO observing run with a hidden Markov model, Phys. Rev. D **95**, 122003 (2017), arXiv:1704.03719 [gr-qc].

[30] B. P. Abbott, R. Abbott, T. D. Abbott, M. R. Abernathy, F. Acernese, K. Ackley, C. Adams, T. Adams, P. Addesso, R. X. Adhikari, and et al., Directional Limits on Persistent Gravitational Waves from Advanced LIGO's First Observing Run, Phys. Rev. Lett. **118**, 121102 (2017), arXiv:1612.02030 [gr-qc].

[31] B. P. Abbott, R. Abbott, T. D. Abbott, S. Abraham, F. Acernese, K. Ackley, C. Adams, R. X. Adhikari, V. B. Adya, C. Affeldt, and et al., Directional limits on persistent gravitational waves using data from Advanced LIGO's first two observing runs, Phys. Rev. D **100**, 062001 (2019), arXiv:1903.08844 [gr-qc].

[32] S. Dhurandhar, B. Krishnan, H. Mukhopadhyay, and J. T. Whelan, Cross-correlation search for periodic gravitational waves, Phys. Rev. D **77**, 082001 (2008), arXiv:0712.1578 [gr-qc].

[33] E. B. Fomalont, B. J. Geldzahler, and C. F. Bradshaw, Scorpius X-1: The Evolution and Nature of the Twin Compact Radio Lobes, ApJ **558**, 283 (2001), arXiv:astro-ph/0104372 [astro-ph].

[34] M. de Kool and U. Anzer, A simple analysis of period noise in binary X-ray pulsars., MNRAS **262**, 726 (1993).

[35] A. Baykal and H. Oegelman, An empirical torque noise and spin-up model for accretion-powered X-ray pulsars., A&A **267**, 119 (1993).

[36] L. Bildsten, D. Chakrabarty, J. Chiu, M. H. Finger, D. T. Koh, R. W. Nelson, T. A. Prince, B. C. Rubin, D. M. Scott, M. Stollberg, B. A. Vaughan, C. A. Wilson, and R. B. Wilson, Observations of Accreting Pulsars, ApJS **113**, 367 (1997), arXiv:astro-ph/9707125 [astro-ph].

[37] A. L. Watts, B. Krishnan, L. Bildsten, and B. F. Schutz, Detecting gravitational wave emission from the known accreting neutron stars, MNRAS **389**, 839 (2008), arXiv:0803.4097 [astro-ph].

[38] A. Mukherjee, C. Messenger, and K. Riles, Accretion-induced spin-wandering effects on the neutron star in Scorpius X-1: Implications for continuous gravitational wave searches, Phys. Rev. D **97**, 043016 (2018), arXiv:1710.06185 [gr-qc].

[39] R. Tenorio, D. Keitel, and A. M. Sintes, Search Methods for Continuous Gravitational-Wave Signals from Unknown Sources in the Advanced-Detector Era, Universe **7**, 474 (2021), arXiv:2111.12575 [gr-qc].

[40] L. White and R. Elliott, A mixed map/mlse receiver for convolutional coded signals transmitted over a fading channel, IEEE Transactions on Signal Processing **50**, 1205 (2002).

[41] S. Paris and C. Jauffret, Frequency line tracking using hmm-based schemes [passive sonar], IEEE Transactions on Aerospace and Electronic Systems **39**, 439 (2003).

[42] The LIGO Scientific Collaboration, the Virgo Collaboration, the KAGRA Collaboration, R. Abbott, T. D. Abbott, S. Abraham, F. Acernese, K. Ackley, A. Adams, C. Adams, and et al., Searches for continuous gravitational waves from young supernova remnants in the early third observing run of Advanced LIGO and Virgo, arXiv e-prints , arXiv:2105.11641 (2021), arXiv:2105.11641 [astro-ph.HE].

[43] J. Bayley, C. Messenger, and G. Woan, Generalized application of the Viterbi algorithm to searches for continuous gravitational-wave signals, Phys. Rev. D **100**, 023006 (2019), arXiv:1903.12614 [astro-ph.IM].

[44] S. Banagiri, L. Sun, M. W. Coughlin, and A. Melatos, Search strategies for long gravitational-wave transients: Hidden Markov model tracking and seedless clustering, Phys. Rev. D **100**, 024034 (2019), arXiv:1903.02638 [astro-ph.IM].

[45] S. Suvorova, P. Clearwater, A. Melatos, L. Sun, W. Moran, and R. J. Evans, Hidden Markov model tracking of continuous gravitational waves from a binary neutron star with wandering spin. II. Binary orbital phase tracking, Phys. Rev. D **96**, 102006 (2017), arXiv:1710.07092 [astro-ph.IM].

[46] S. Suvorova, L. Sun, A. Melatos, W. Moran, and R. J. Evans, Hidden Markov model tracking of continuous gravitational waves from a neutron star with wandering spin, Phys. Rev. D **93**, 123009 (2016), arXiv:1606.02412 [astro-ph.IM].

[47] C. Messenger, H. J. Bulten, S. G. Crowder, V. Dergachev, D. K. Galloway, E. Goetz, R. J. G. Jonker, P. D. Lasky, G. D. Meadors, A. Melatos, S. Premachandra, K. Riles, L. Sammut, E. H. Thrane, J. T. Whelan, and Y. Zhang, Gravitational waves from Scorpius X-1: A comparison of search methods and prospects for detection with advanced detectors, Phys. Rev. D **92**, 023006 (2015), arXiv:1504.05889 [gr-qc].

[48] A.Viterbi, Error bounds for convolutional codes and an asymptotically optimum decoding algorithm, IEEE Transactions on Information Theory **13**, 260 (1967).

[49] P. Jaranowski, A. Królak, and B. F. Schutz, Data analysis of gravitational-wave signals from spinning neutron stars: The signal and its detection, Phys. Rev. D **58**, 063001 (1998), arXiv:gr-qc/9804014 [gr-qc].

[50] R. Prix and B. Krishnan, Targeted search for continuous gravitational waves: Bayesian versus maximum-likelihood statistics, Classical and Quantum Gravity **26**, 204013 (2009), arXiv:0907.2569 [gr-qc].

[51] L. Wang, D. Steeghs, D. K. Galloway, T. Marsh, and J. Casares, Precision Ephemerides for Gravitational-wave Searches - III. Revised system parameters of Sco X-1, MNRAS **478**, 5174 (2018), arXiv:1806.01418 [astro-ph.HE].

[52] C. F. Bradshaw, E. B. Fomalont, and B. J. Geldzahler, High-Resolution Parallax Measurements of Scorpius X-1, ApJ **512**, L121 (1999).

[53] P. Leaci and R. Prix, Directed searches for continuous gravitational waves from binary systems: Parameter-space metrics and optimal Scorpius X-1 sensitivity, Phys. Rev. D **91**, 102003 (2015), arXiv:1502.00914 [gr-qc].

[54] R. Prix, LIGO Report T0900149 (June 2011).

[55] LIGO Scientific Collaboration, LIGO Algorithm Library - LALSuite, free software (GPL) (2018).

[56] J. Zweizig and K. Riles, LIGO-T2000384-v4: Information on self-gating of h(t) used in O3 continuous-wave and stochastic searches.

[57] B. P. Abbott, R. Abbott, T. D. Abbott, S. Abraham, F. Acernese, K. Ackley, C. Adams, V. B. Adya, C. Affeldt, M. Agathos, and et al., A guide to LIGO-Virgo detector noise and extraction of transient gravitational-wave signals, Classical and Quantum Gravity **37**, 055002 (2020), arXiv:1908.11170 [gr-qc].

[58] G. Vajente, Y. Huang, M. Isi, J. C. Driggers, J. S. Kissel, M. J. Szczepańczyk, and S. Vitale, Machine-learning nonstationary noise out of gravitational-wave detectors, Phys. Rev. D **101**, 042003 (2020), arXiv:1911.09083 [gr-qc].

[59] B. P. Abbott, R. Abbott, T. D. Abbott, M. R. Abernathy, F. Acernese, K. Ackley, C. Adams, T. Adams, P. Addesso, R. X. Adhikari, and et al., Upper Limits on the Stochastic Gravitational-Wave Background from Advanced LIGO's First Observing Run, Phys. Rev. Lett. **118**, 121101 (2017), arXiv:1612.02029 [gr-qc].

[60] P. B. Covas, A. Effler, E. Goetz, P. M. Meyers, A. Neunzert, M. Oliver, B. L. Pearlstone, V. J. Roma, R. M. S. Schofield, V. B. Adya, and et al., Identification and mitigation of narrow spectral artifacts that degrade searches for persistent gravitational waves in the first two observing runs of Advanced LIGO, Phys. Rev. D **97**, 082002 (2018), arXiv:1801.07204 [astro-ph.IM].

[61] E. Goetz, A. Neunzert, K. Riles, A. Matas, S. Kandhasamy, J. Tasson, C. Barschaw, H. Middleton, S. Hughey, L. Mueller, J. Heinzel, J. Carlin, A. Vargas, and I. Hollows, T2100200-v1: O3 lines and combs in found in self-gated C01 data.

[62] R. Abbott, T. D. Abbott, S. Abraham, F. Acernese, K. Ackley, A. Adams, C. Adams, R. X. Adhikari, V. B. Adya, C. Affeldt, and et al., Search for anisotropic gravitational-wave backgrounds using data from Advanced LIGO and Advanced Virgo's first three observing runs, Phys. Rev. D **104**, 022005 (2021), arXiv:2103.08520 [gr-qc].

[63] H. Ritter and U. Kolb, Catalogue of cataclysmic binaries, low-mass X-ray binaries and related objects (Seventh edition), A&A **404**, 301 (2003), arXiv:astro-ph/0301444 [astro-ph].

[64] L. Sammut, Gravitational waves from low-mass X-ray binaries: a search for Scorpius X-1, Ph.D. thesis, The University of Melbourne (2015).